Strong magnetic field induces superconductivity in a Weyl semimetal

Baruch Rosenstein,[1,*] B. Ya. Shapiro,[2,†] Dingping Li,[3,4,‡] and I. Shapiro[2]
[1]*Department of Electrophysics, National Chiao Tung University, Hsinchu 30050, Taiwan, Republic of China*
[2]*Department of Physics, Bar-Ilan University, 52900 Ramat-Gan, Israel*
[3]*School of Physics, Peking University, Beijing 100871, China*
[4]*Collaborative Innovation Center of Quantum Matter, Beijing 100871, China*
(Received 14 August 2017; revised manuscript received 8 December 2017; published 29 December 2017)

Microscopic theory of the normal-to-superconductor coexistence line of a multiband Weyl superconductor subjected to magnetic field is constructed. It is shown that the Weyl semimetal that is nonsuperconducting or having a small critical temperature T_c at zero field might become a superconductor at higher temperatures when the magnetic field is tuned to a series of quantized values H_n. The pairing occurs on Landau levels. It is argued that the phenomenon is detectable much easier in Weyl semimetals than in parabolic band metals since the quantum limit already has been approached in several Weyl materials. The effect of Zeeman coupling leading to splitting of the reentrant superconducting regions on the magnetic phase diagram is considered. An experimental signature of the superconductivity on Landau levels is the reduction of magnetoresistivity. This has been observed already in Cd_3As_2 and several other compounds. The novel kind of quantum oscillations of magnetoresistance detected in $ZrTe_5$ is discussed along these lines.

DOI: 10.1103/PhysRevB.96.224517

I. INTRODUCTION

Conventional superconductivity arises from pairing of electrons in the vicinity of the Fermi surface since the phonon mediated attraction is effective only when the electron's energy is within a shell of the Debye energy width, $\hbar\Omega$ of orders of several hundreds of kelvin, see Fig. 1. Within the BCS theory (in the adiabatic limit) the order parameter, $\Delta \sim T_c$, depends exponentially on the density of states (DOS) at Fermi level $D(\mu)$ so that in order to enhance the tendency for superconductivity, one should use any means to boost the density of states within this narrow shell. In quantum systems there is an obvious way to locally boost the DOS—quantization. Thus a natural mean to concentrate the spectral weight is a strong magnetic field that causes Landau quantization. The best known example of this phenomenon is the two-dimensional electron gas (2DEG) in a magnetic field where the DOS can be tuned to "infinity" at certain values of magnetic fields and the quantum Hall effect became visible.

In principle, one can imagine that strong magnetic field can enhance superconductivity as well if the quantum limit [when the Fermi surface crosses the lowest Landau levels (LLs)] is reached. At first glance there are two immediate problems with this scenario. First the magnetic field generally breaks the Cooper pairs due to the orbital instability that leads [1] to suppression of superconductivity at H_{c2}. Second, the direct (Zeeman) coupling of the magnetic field to the electron's spin also leads (for the singlet pairing) to the Chandrasekhar-Klogston [2] pair breaking at H_p. However it was predicted in the 1980s of the past century (see Refs. [3–5] and references therein) that paradoxically superconductivity can reappear on the LLs at fields far above H_{c2}. Although the superconductivity enhancement can occur at any LL, it is stable against perturbations only near the "quantum limit" in which the lowest LL crosses the Fermi energy μ. The condition for that, $\mu \sim \hbar\omega_c^p$, however restricts the choice of material to those with extremely low electron densities. Even for 100 T the Fermi level should be just 10 meV.

In conventional metallic superconductors, even at $H_{c2} = \Phi_0/2\pi\xi^2$ (where ξ is the coherence length at zero temperature and Φ_0 is the flux quantum), the effect of the Landau quantization of the electron motion is negligible. For a metal with effective mass m^*, the separation between (equidistant) Landau levels is $\hbar\omega_c^p = \hbar eH/m^*c$. For typical values of the field $H_{c2} = 3$ T and effective mass $m^* \sim m_e$, the level spacing is 4 K, much smaller than $2\hbar\Omega$. Therefore, to take advantage of the Landau quantization effect on superconductivity, one should consider a superstrong magnetic field of thousands of teslas. The estimate however is based on the assumption of the parabolic dispersion relation of the normal electrons (or holes).

Recently a new class of 2D and three-dimensional (3D) multiband materials with qualitatively different band structures near the Fermi level was discovered [6–11]—Weyl (Dirac) semimetals (WSMs). Unlike in conventional semimetals with several quasiparticle and hole bands, in WSMs Dirac points occur due to the band inversion near the Fermi level. WSMs are characterized by the linear dispersion relation $\varepsilon = vp$, and in many of them the chemical potential is tunable and small. An even more important fact for pairing is that their interband tunneling is dominant. In some of these novel materials conventional phonon-mediated superconductivity with T_c up to 20 K (under pressure) with H_{c2} of several teslas was achieved [7,8]. Although the mechanism of superconductivity is that these materials do not differ much from the low-T_c metals [12,13], the position of the LLs does. The notion of the effective mass does not apply for this essentially nonparabolic dispersion relation, and LLs generally are no longer equidistant [6], see Fig. 1. This raises the possibility that the Landau quantum limit is achievable much easier in this case [9]. The first LL that appears at $\hbar\omega_c = v\sqrt{2\hbar eH/c}$ should be equal

*baruchro@hotmail.com
†shapib@mail.biu.ac.il
‡lidp@pku.edu.cn

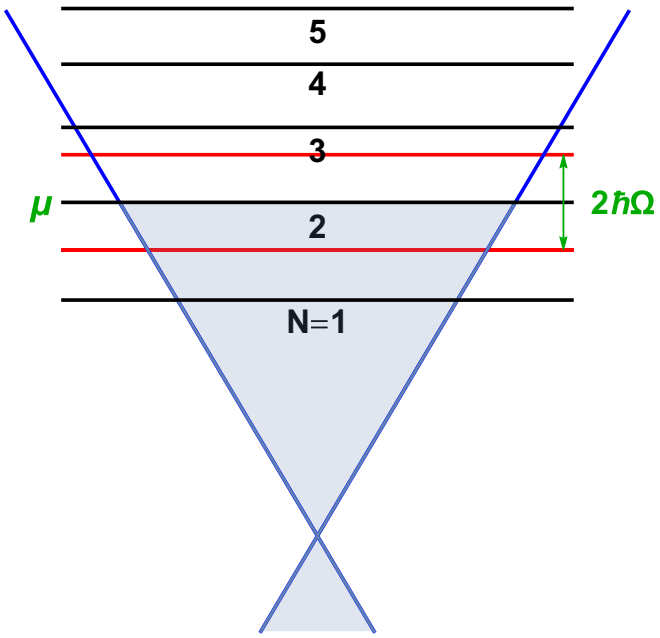

FIG. 1. Set of Landau levels in Weyl semimetals. Pairing due to phonons occurs in the energy shell of the Debye energy width $\hbar\Omega$ around the Fermi-level μ.

to μ counted from the Dirac point. For typical values of $v = 10^8$ cm/s and $H = 100$ T, now one obtains $\mu = 0.4$ eV that favorably compares with the previous estimate of 10 meV in a "conventional" parabolic band. The condition for the superconductivity enhancement in WSMs is thus qualitatively different, and the quantum limit condition becomes $\omega_c\hbar \sim 2\hbar\Omega$. A more quantitative estimate and comparison between the conventional materials and the WSM are made below. Therefore it is important to extend the BCS-type theory to the case of multiband semimetals, such as the WSM. The extension of conventional Gor'kov-Eliashberg approach in strong magnetic fields [3–5] to multiband semimetals by no means is trivial. For two parabolic (one quasiparticle and one hole) bands it was performed in Ref. [14]. Since in WSMs the ratio $\mu/\hbar\Omega$ is relatively small, an important additional issue is the role of the retardation effects of the phonon-mediated pairing in order to remain within the bounds of the adiabatic approximation.

In this paper the effect of the phonon-mediated pairing in strong magnetic fields (including the quantum limit) in Weyl semimetals is developed in a wide range of temperatures and magnetic fields. The simplest model necessarily contains four (sub) bands (two Weyl subbands and two magnetically split spin subbands due to Zeeman coupling). The magnetic phase diagram consists of a series of superconducting domes in addition to the conventional $H_{c2}(T)$ line. Recent experiments [9] on Cd_3As_2 in fields up to 52 T are reinterpreted as possible candidates for reentrant superconductivity at $N = 2,3$ Landau levels at 25 and 46 T. It is interesting to note that the upper bound on superconductivity at zero fields in this material is 3 K. Retardation effects of the phonon-mediated pairing is discussed and taken into account phenomenologically.

The paper is organized as follows. The effect of reentrant superconductivity at very high magnetic fields is more pronounced in two dimensions, so a sufficiently general 2D WSM model is defined in Sec. II. The superconductor-normal phase-transition line in 2D WSMs in high magnetic fields is derived in Sec. III. The phase diagram of superconductivity on Landau levels is extended to Zeeman coupling and to the anisotropic 3D WSMs in Sec. IV. Comparison with recent experiments, discussions, and conclusions is the subject of Sec. V.

II. PHONON-MEDIATED SUPERCONDUCTIVITY IN WSMS IN STRONG MAGNETIC FIELDS

A. Pairing in the WSM under magnetic fields

A Weyl material typically possesses several sublattices. We exemplify the effect of the WSM band structure on superconductivity using the simplest model with just two sublattices denoted by $\alpha = 1,2$. The effective electron-electron attraction due to the electron-phonon coupling overcomes the Coulomb repulsion and induces pairing. Typically in WSMs there are numerous bands. We assume that different valleys are paired independently and drop all the valley indices (including chirality, multiplying the density of states by $2N_f$). To simplify notations, we therefore consider just one spinor (left, for definiteness), the following Weyl Hamiltonian [13,15],

$$K = \int_{\mathbf{r}} \psi_\alpha^{s\dagger}(\mathbf{r})\left\{-i\hbar v\left(D_x\sigma_{\alpha\beta}^x + D_y\sigma_{\alpha\beta}^y\right) - \mu\delta_{\alpha\beta}\right\}\psi_\beta^s(\mathbf{r}). \quad (1)$$

Here v is the Fermi velocity assumed isotropic on the plane x-y perpendicular to the applied magnetic field (assumed isotropic, generalized later to an anisotropic 3D WSM). The chemical potential is denoted by μ—the chemical potential. Pauli matrices σ operate in the sublattice space (the indices α,β will be termed the pseudospin projections), and s is the spin projection. A magnetic field appears in the covariant derivatives via the vector potential $D_i = \nabla^i - i\frac{e}{\hbar c}A_i$. Here $\mathbf{A}$ is the vector potential.

Furthermore, we assume the local density-density interaction Hamiltonian [16],

$$V = \frac{g^2}{2}\int_{\mathbf{r}} \psi_\alpha^{+\uparrow}(\mathbf{r})\psi_\alpha^{\downarrow}(\mathbf{r})\psi_\beta^{\downarrow+}(\mathbf{r})\psi_\beta^{\uparrow}(\mathbf{r}), \quad (2)$$

ignoring the Coulomb repulsion (that as usual is accounted for by a pseudopotential so that g is the electron-phonon coupling). It is important that the interaction has a cutoff Debye frequency Ω so that it is active in an energy shell of width $2\hbar\Omega$ around the Fermi level [16]. We will discuss a more realistic dependence on frequency in Sec. III.

B. Matsubara Green's functions and Gor'kov equations

Finite-temperature properties of the superconducting condensate are described by the normal and the anomalous Matsubara Green's functions (GFs) [16],

$$\begin{aligned} G_{\alpha\beta}^{ts}(\mathbf{r}\tau,\mathbf{r}'\tau') &= -\left\langle T\psi_\alpha^t(\mathbf{r}\tau)\psi_\beta^{\dagger s}(\mathbf{r}'\tau')\right\rangle, \\ F_{\alpha\beta}^{ts}(\mathbf{r}\tau,\mathbf{r}'\tau') &= \left\langle T\psi_\alpha^t(\mathbf{r}\tau)\psi_\beta^s(\mathbf{r}'\tau')\right\rangle, \\ F_{\alpha\beta}^{+ts}(\mathbf{r}\tau,\mathbf{r}'\tau') &= \left\langle T\psi_\alpha^{\dagger t}(\mathbf{r}\tau)\psi_\beta^{\dagger s}(\mathbf{r}'\tau')\right\rangle, \end{aligned} \quad (3)$$

with the spin ansatz,

$$G^{ts}_{\alpha\beta}(\mathbf{r}\tau,\mathbf{r}'\tau') = \delta^{ts}G_{\alpha\beta}(\mathbf{r},\mathbf{r}',\tau-\tau'),$$
$$F^{ts}_{\alpha\beta}(\mathbf{r}\tau,\mathbf{r}'\tau') = -\varepsilon^{ts}F_{\alpha\beta}(\mathbf{r},\mathbf{r}',\tau-\tau'),$$
$$F^{+ts}_{\alpha\beta}(\mathbf{r}\tau,\mathbf{r}'\tau') = \varepsilon^{ts}F^{+}_{\alpha\beta}(\mathbf{r},\mathbf{r}',\tau-\tau'). \quad (4)$$

Here the Planck constant is set to $\hbar = 1$. Using the Fourier transform,

$$G_{\gamma\kappa}(\mathbf{r},\tau) = T\sum_s \exp[-i\omega_s\tau]G_{\gamma\kappa}(\omega,\mathbf{r}), \quad (5)$$

with fermionic Matsubara frequencies $\omega_s = 2\pi T(s+1/2)$, one obtains the set of Gor'kov equations from equations of operator motion, see Refs. [13,17] generalized to include a magnetic field,

$$i\omega G_{\gamma\kappa}(\mathbf{r},\mathbf{r}',\omega) + iv\mathbf{D}^i_{\mathbf{r}}\sigma^i_{\gamma\beta}G_{\beta\kappa}(\mathbf{r},\mathbf{r}',\omega) + \mu G_{\gamma\kappa}(\mathbf{r},\mathbf{r}',\omega) + \Delta_{\alpha\gamma}(\mathbf{r},0)F^{+}_{\alpha\kappa}(\mathbf{r},\mathbf{r}',\omega) = \delta^{\gamma\kappa}\delta(\mathbf{r}-\mathbf{r}'),$$
$$-i\omega F^{+}_{\gamma\kappa}(\mathbf{r},\mathbf{r}',\omega) - iv\mathbf{D}^i_{\mathbf{r}}\sigma^i_{\alpha\gamma}F^{+}_{\alpha\kappa}(\mathbf{r},\mathbf{r}',\omega) + \mu F^{+}_{\gamma\kappa}(\mathbf{r},\mathbf{r}',\omega) - \Delta^{*}_{\alpha\gamma}(\mathbf{r},0)G_{\alpha\kappa}(\mathbf{r},\mathbf{r}',\omega) = 0. \quad (6)$$

It will be shown that the singlet pairing pseudospin ansatz $\Delta_{\alpha\gamma} \equiv \sigma^x_{\alpha\gamma}\Delta$ obeys the Pauli principle. The gap function consequently reads: $\Delta = \frac{1}{2}\mathrm{Tr}[\sigma^x\widehat{\Delta}]$. Notice, that in contrast to conventional metals with parabolic dispersion law, in the case of the Weyl semimetals the second Gor'kov equation, Eq. (6), contains transposed Pauli matrices for isospins. The applicability of the mean-field approach in a purely 2D model have been discussed widely [5] since (logarithmic) infrared divergences appear in corrections to the approximation. The corrections of the long-range charge-density waves instability are assumed to be cut off by the finite size of the sample, etc.

III. THE TRANSITION LINE

In this section the superconductor-normal phase-transition line in high magnetic fields is determined. The line breaks into a set of disconnected segments since in certain cases the superconductivity reappears when a Landau level crosses the Fermi surface.

A. Linearization of the Gor'kov equations near the transition line

Near the normal-to-superconducting transition line the gap Δ is small, and the set of the Gor'kov equations (6) can be linearized. In this case the gap equation describing the critical curve $H_{c2}(T)$ has the form, see Ref. [17] for details,

$$\Delta(\mathbf{r}) = \frac{g^2}{2}T\sum_\omega\int_{\mathbf{r}'}\Delta^{*}(\mathbf{r}')\sigma^x_{\kappa\beta}G^2_{\beta\gamma}(\mathbf{r}',\mathbf{r})\sigma^x_{\gamma\alpha}G^1_{\alpha\kappa}(\mathbf{r},\mathbf{r}')$$
$$= \frac{g^2}{2}\sum_\omega\int_{\mathbf{r}'}\Delta^{*}(\mathbf{r}')$$
$$\times\begin{pmatrix} G^2_{22}(\mathbf{r}',\mathbf{r})G^1_{11}(\mathbf{r},\mathbf{r}') + G^2_{11}(\mathbf{r}',\mathbf{r})G^1_{22}(\mathbf{r},\mathbf{r}') \\ +G^2_{12}(\mathbf{r}',\mathbf{r})G^1_{12}(\mathbf{r},\mathbf{r}') + G^2_{21}(\mathbf{r}',\mathbf{r})G^1_{21}(\mathbf{r},\mathbf{r}')\end{pmatrix}. \quad (7)$$

Here the normal GF is obtained from

$$[iv\mathbf{D}_{\mathbf{r}}\cdot\sigma_{\gamma\beta} + (i\omega+\mu)\delta_{\gamma\beta}]G^1_{\beta\kappa}(\mathbf{r},\mathbf{r}') = \delta^{\gamma\kappa}\delta(\mathbf{r}-\mathbf{r}'), \quad (8)$$

whereas a quantity $\overline{G}_{\beta\gamma}$ (an auxiliary function associated with G via a product of an axis reflection and time reversal) obeys a *different* equation,

$$\left[-iv\mathbf{D}_{\mathbf{r}}\cdot\sigma^t_{\gamma\beta} + (-i\omega+\mu)\delta_{\gamma\beta}\right]G^2_{\beta\kappa}(\mathbf{r}',\mathbf{r}) = \delta^{\gamma\kappa}\delta(\mathbf{r}-\mathbf{r}'). \quad (9)$$

Here σ^t is the transposed Pauli matrix that replaces σ in the customary normal-state equation Eq. (8).

In the uniform magnetic field the GF can be written (in the symmetric gauge $\mathbf{A} = \frac{1}{2}\mathbf{H}\times\mathbf{r}$) in the following form:

$$G^1_{\beta\kappa}(\mathbf{r},\mathbf{r}') = \exp\left[-i\frac{xy'-yx'}{2l^2}\right]g^1_{\beta\kappa}(\mathbf{r}-\mathbf{r}'),$$
$$G^2_{\beta\kappa}(\mathbf{r}',\mathbf{r}) = \exp\left[-i\frac{xy'-yx'}{2l^2}\right]g^2_{\beta\kappa}(\mathbf{r}'-\mathbf{r}). \quad (10)$$

Here $l^2 = c/eH$ is the magnetic length. This phase ansatz indeed works. Substituting it into Eqs. (8) and (9), respectively, the variables separate

$$\{(i\omega+\mu)\delta_{\gamma\beta} - v\Pi\cdot\sigma_{\gamma\beta}\}g^1_{\beta\kappa}(\mathbf{r}-\mathbf{r}') = \delta^{\gamma\kappa}\delta(\mathbf{r}-\mathbf{r}'), \quad (11)$$

$$\left\{(-i\omega+\mu)\delta_{\gamma\beta} + v\Pi\cdot\sigma^t_{\gamma\beta}\right\}g^2_{\beta\kappa}(\mathbf{r}'-\mathbf{r}) = \delta^{\gamma\kappa}\delta(\mathbf{r}-\mathbf{r}'). \quad (12)$$

Here the ladder operators are defined as

$$\Pi_x = -i\frac{\partial}{\partial\rho_x} + \frac{1}{2l^2}\rho_y, \quad \Pi_y = -i\frac{\partial}{\partial\rho_y} - \frac{1}{2l^2}\rho_x, \quad (13)$$

with the relative distance denoted by $\rho = \mathbf{r}-\mathbf{r}'$.

These equations are solved by expansion in the basis of eigenfunctions of harmonic oscillator in Appendix A. The resulting normal GFs in terms of generalized Laguerre polynomials are as follows:

$$g^1_{11}(\rho) = \frac{(i\omega+\mu)}{2\pi l^2}\exp\left[-\frac{\rho^2}{4l^2}\right]\sum_{n=0}\frac{L_n[\rho^2/2l^2]}{(i\omega+\mu)^2-\omega_c^2(n+1)},$$
$$g^1_{21}(\rho) = -\frac{iv\rho e^{i\theta}}{2\pi l^4}\exp\left[-\frac{\rho^2}{4l^2}\right]\sum_{n=1}\frac{L^1_{n-1}[\rho^2/2l^2]}{(i\omega+\mu)^2-\omega_c^2(n+1)},$$
$$g^1_{22}(\rho) = \frac{(i\omega+\mu)}{2\pi l^2}\exp\left[-\frac{\rho^2}{4l^2}\right]\sum_{n=0}\frac{L_n[\rho^2/2l^2]}{(i\omega+\mu)^2-\omega_c^2 n},$$
$$g^1_{12}(\rho) = -\frac{iv\rho e^{-i\theta}}{2\pi l^4}\exp\left[-\frac{\rho^2}{4l^2}\right]\sum_{n=1}\frac{L^1_n[\rho^2/2l^2]}{(i\omega+\mu)^2-\omega_c^2 n}. \quad (14)$$

Here the cyclotron frequency in the WSM is denoted by $\omega_c^2 = 2v^2/l^2$, and θ is the polar angle of ρ. Similarly the associate

GFs are as follows:

$$g^2_{11}(-\rho) = \frac{-i\omega+\mu}{2\pi l^2}\exp\left[-\frac{\rho^2}{4l^2}\right]\sum_{n=0}\frac{L_n[\rho^2/2l^2]}{(-i\omega+\mu)^2-\omega_c^2 n},$$

$$g^2_{12}(-\rho) = \frac{iv\rho e^{i\theta}}{2\pi l^4}\exp\left[-\frac{\rho^2}{4l^2}\right]\sum_{n=1}\frac{L^1_{n-1}[\rho^2/2l^2]}{(-i\omega+\mu)^2-\omega_c^2(n+1)},$$

$$g^2_{21}(-\rho) = \frac{iv\rho e^{-i\theta}}{2\pi l^4}\exp\left[-\frac{\rho^2}{4l^2}\right]\sum_{n=1}\frac{L^1_{n}[\rho^2/2l^2]}{(-i\omega+\mu)^2-\omega_c^2 n},$$

$$g^2_{22}(-\rho) = \frac{-i\omega+\mu}{2\pi l^2}\exp\left[-\frac{\rho^2}{4l^2}\right] \times\sum_{n=0}\frac{L_n[\rho^2/2l^2]}{(-i\omega+\mu)^2-\omega_c^2(n+1)}. \quad (15)$$

Now we are ready to return to the gap equation at criticality.

B. Ansatz for the gap function and the angle integration

Substituting the phase factors of the GF from Eq. (10) into the gap equation Eq. (7) one obtains

$$\Delta(\mathbf{r}) = \frac{g^2T}{2}\sum_\omega\int_{\mathbf{r}'}\exp\left[-i\frac{xy'-yx'}{l^2}\right]\Delta^*(\mathbf{r}') \times\begin{pmatrix} g^2_{22}(-\rho)g^1_{11}(\rho)+g^2_{11}(-\rho)g^1_{22}(\rho) \\ +g^2_{12}(-\rho)g^1_{12}(\rho)+g^2_{21}(-\rho)g^1_{21}(\rho)\end{pmatrix}. \quad (16)$$

Adopting the Gaussian ansatz for the gap function,

$$\Delta(\mathbf{r}) = \exp[-r^2/2l^2] \quad (17)$$

used extensively in calculations since the seminal work [1], and substituting the above explicit expressions for the GF, one obtains

$$1 = \frac{g^2T}{8\pi^2 l^4}\sum_\omega\int_0^\infty\rho\,d\rho\int_{\theta=0}^{2\pi}\exp\left[\frac{r\rho}{l^2}e^{i\theta}\right]\exp[-2u]S(u,\omega), \quad (18)$$

where the integrals have been shifted to $\rho = \mathbf{r}-\mathbf{r}'$. The scalar function S depends on the absolute value of ρ only so that the dimensionless variable $u = \rho^2/2l^2$ is used instead. It is a double sum over Landau levels,

$$S(u,\omega) = (\omega^2+\mu^2)\sum_{n,m=0}^\infty\left\{\frac{L_n[u]L_m[u]}{\left[(-i\omega+\mu)^2-\omega_c^2(n+1)\right]\left[(i\omega+\mu)^2-\omega_c^2(m+1)\right]}+\frac{L_n[u]L_m[u]}{\left[(-i\omega+\mu)^2-\omega_c^2 n\right]\left[(i\omega+\mu)^2-\omega_c^2 m\right]}\right\}$$
$$+\omega_c^2\sum_{n,m=1}^\infty\left\{\frac{uL^1_{n-1}[u]L^1_m[u]}{\left[(-i\omega+\mu)^2-\omega_c^2(n+1)\right]\left[(i\omega+\mu)^2-\omega_c^2 m\right]}+\frac{uL^1_n[u]L^1_{m-1}[u]}{\left[(-i\omega+\mu)^2-\omega_c^2 n\right]\left[(i\omega+\mu)^2-\omega_c^2(m+1)\right]}\right\}. \quad (19)$$

The integral over θ is just [18] 2π so that the gap equation at criticality takes the form

$$1 = \frac{g^2T}{4\pi l^2}\sum_\omega\int_{u=0}^\infty\exp[-2u]S(u,\omega). \quad (20)$$

In what follows the integral over u and the sum over the Matsubara frequencies are performed explicitly and the equation used to investigate the effect of Landau quantization of superconductivity in a WSM. Using the integrals over the product of generalized Laguerre polynomials [18],

$$\int_0^\infty du\ \exp(-2u)L_n(u)L_m(u) = \frac{(m+n)!}{2^{m+n+1}m!n!},$$
$$\int_0^\infty u\,du\ \exp(-2u)L^1_{n-1}(u)L^1_m(u) = \frac{(m+n)!}{2^{m+n+1}m!(n-1)!}, \quad (21)$$

the gap equation takes the form

$$\frac{1}{\lambda} = \frac{\overline{\omega}_c^2}{4\overline{\mu}}\sum_s\left\{\begin{array}{l}\sum_{n,m=0}\frac{(m+n)!}{2^{m+n}m!n!}\left(\frac{\overline{\omega}_s^2+\overline{\mu}^2}{\left[(-i\overline{\omega}_s+\overline{\mu})^2-\overline{\omega}_c^2(n+1)\right]\left[(i\overline{\omega}_s+\mu)^2-\overline{\omega}_c^2(1+n)\right]}+\frac{\overline{\omega}_s^2+\overline{\mu}^2}{\left[(-i\overline{\omega}_s+\overline{\mu})^2-\overline{\omega}_c^2 n\right]\left[(i\overline{\omega}_s+\overline{\mu})^2-\overline{\omega}_c^2 m\right]}\right) \\ +\sum_{n,m=1}\frac{(m+n)!}{2^{m+n}m!n!}\left(\frac{n\overline{\omega}_c^2}{\left[(-i\overline{\omega}_s+\overline{\mu})^2-\overline{\omega}_s^2(n+1)\right]\left[(i\overline{\omega}_s+\overline{\mu})^2-\overline{\omega}_c^2 m\right]}+\frac{m\overline{\omega}_c^2}{\left[(-i\overline{\omega}_s+\overline{\mu})^2-\overline{\omega}_c^2 n\right)\left[(i\overline{\omega}_s+\overline{\mu})^2-\overline{\omega}_c^2(1+m)\right]}\right)\end{array}\right\}, \quad (22)$$

where the effective dimensionless electron-electron coupling $\lambda = g^2\mu/4\pi v^2$. It is also convenient to scale μ and ω_c by the temperature $\overline{\mu} = \mu/T$, $\overline{\omega}_c = \omega_c/T$. After the summation over the Matsubara frequency, one obtains, separating the zero LL ($n=0$) from the rest,

$$\frac{1}{\lambda} = \frac{\overline{\omega}_c^2}{4\overline{\mu}}\left\{\sum_{n,m}\frac{(m+n)!}{2^{m+n+1}}\frac{f[n]f[m]}{m!n!}s_{nm}+\sum_n\frac{f[n]f[0]}{2^n}s_n+\frac{f[0]^2}{2}s\right\}, \quad (23)$$

where $f(n)$ will be discussed in the next subsection. The separation is required since the expressions in Appendix B are ambiguous for $n = 0$ and should be defined using l'Hôpital's rule. The $n,m > 0$ part (free of the ambiguous terms) is as follows:

$$s_{nm} = A\left[\overline{\omega}_c^2(n+1),\overline{\omega}_c^2(m+1)\right] + A\left[\overline{\omega}_c^2 n,\overline{\omega}_c^2 m\right] + \left(\begin{array}{c} \overline{\mu}^2 B\left[\overline{\omega}_c^2(n+1),\overline{\omega}_c^2(m+1)\right] + \overline{\mu}^2 B\left[\overline{\omega}_c^2 n,\overline{\omega}_c^2 m\right] \\ +n\overline{\omega}_c^2 B\left[\overline{\omega}_c^2(n+1),\overline{\omega}_c^2 m\right] + m\overline{\omega}_c^2 B\left[\overline{\omega}_c^2 n,\overline{\omega}_c^2(m+1)\right] \end{array}\right). \quad (24)$$

The mixed zero-nonzero LL ($n = 0$, $m > 0$) part is

$$s_n = A\left[\overline{\omega}_c^2(n+1),\overline{\omega}_c^2\right] + A\left[\overline{\omega}_c^2 n,0\right] + \overline{\mu}^2 B\left[\overline{\omega}_c^2(n+1),\overline{\omega}_c^2\right] + \overline{\mu}^2 B\left[\overline{\omega}_c^2 n,0\right], \quad (25)$$

whereas the purely zero LL contribution,

$$s = A\left[\overline{\omega}_c^2,\overline{\omega}_c^2\right] + A[0,0] + \overline{\mu}^2 B\left[\overline{\omega}_c^2,\overline{\omega}_c^2\right] + \overline{\mu}^2 B[0,0]. \quad (26)$$

The explicit form of functions A and B is given in Appendix B. It is shown there that the functions are finite for any value of magnetic field and temperature $T > 0$. The sum is computed numerically.

C. Phonon retardation effects

Usually within the BCS approach, the interaction is approximated not just by a contact in space and a step functionlike cutoff,

$$\mu - \hbar\Omega < \hbar\omega_c\sqrt{n} < \mu + \hbar\Omega, \quad (27)$$

see Fig. 1. Therefore the sums over Landau levels in Eq. (23) are restricted. The approximation is not good enough for our purposes since, when crossing a Landau level by increasing the field infinitesimally, the result of the summation in the quantum regime jumps by a finite amount, such as Hall conductivity in 2DEG. This is unphysical since the step function dependence is just an approximation of a more realistic second-order effective electron interaction due to phonon exchange.

Neglecting the dispersion of the optical phonon, the sharp cutoff will be replaced by the Lorenzian function of $\omega_s = \pi T(2s+1)/\hbar$,

$$V(s,p) = \frac{g^2\Omega^2}{\Omega^2 + \omega_s^2}. \quad (28)$$

In our scaled units the summation over the Landau levels comes with a weight function,

$$f(n) = \frac{\Omega^2}{\Omega^2 + (\omega_c\sqrt{n} - \mu/\hbar)^2}. \quad (29)$$

The remaining sums over the Landau levels in Eq. (24) were performed numerically to determine the normal-superconductor transition line.

D. The fragmented transition line

The magnetic phase diagram is the main result of the present paper. Although in experiments the material parameter λ is fixed, whereas the temperature and magnetic field (or both) are external parameters, it is more convenient to calculate the critical value of λ as a function of temperature and magnetic field. In Fig. 2 the inverse effective electron-electron coupling λ^{-1} is plotted as a function of magnetic field. Curves correspond to three temperatures $\hbar\Omega/200$, $\hbar\Omega/50$, and $\hbar\Omega/20$, whereas the wide range of magnetic fields extends up to $25\hbar c\Omega^2/ev^2$. The value of the chemical potential is chosen to be $\mu = 5\hbar\Omega$. For concreteness (and to facilitate a discussion of an experiment on Cd_3As_2) we use typical values of the Debye frequency $\Omega = 400$ K and the Fermi velocity $v = 10^8$ cm/s so that temperatures and fields in Fig. 2 are given in kelvins and teslas, respectively. The dashed lines mark the cases of a weak $\lambda = 0.2$, an intermediate $\lambda = 0.33$, and a relatively strong-coupling $\lambda = 1$.

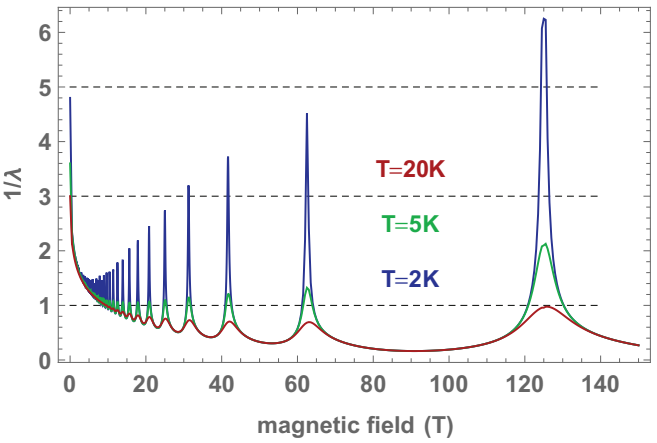

FIG. 2. The inverse effective electron coupling is presented for three temperatures $\hbar\Omega/200$, $\hbar\Omega/50$, and $\hbar\Omega/20$ in a wide range of magnetic fields up to $15\hbar c\Omega^2/ev^2$. The value of the chemical potential is chosen as $\mu = 5\hbar\Omega$.

For the weak coupling the conventional H_{c2} does not appear in the figure since the critical temperature is below 2 K. The only superconducting dome appears at the quantum limit with Cooper pairs made on the lowest LL only. At the intermediate coupling the conventional $H_{c2} = 2$ T does appear (around 4 K), but now there are four additional superconducting domes at Landau levels $N = 1$–4. At the strong coupling regular H_{c2} around 12 T is clearly the dominant feature with numerous domes appearing at $T = 2$ K. The problematic issue of rigorously defining the semiclassical notion of H_{c2} from the microscopic calculation is the same as for the conventional superconductor (parabolic band) [3]. Of course yet at lower temperatures more domes appear.

In Fig. 3 the phase diagram in H-T is presented for the same three values of the effective electron-electron couplings.

The superconducting domes on the Landau levels clearly are seen as gray areas. Generally they become very narrow as the LL index N grows at low temperatures and at weak couplings. The WSM in which we suspect that the high magnetic-field superconducting domes were observed (see Sec. IV) are anisotropic 3D WSMs. In addition at fields as large as 50–60 T applied in recent experiments [9,15] the Zeeman coupling to spin cannot be ignored. Therefore the next section is devoted to generalizations of the direct coupling to the electron spin and 3D WSMs.

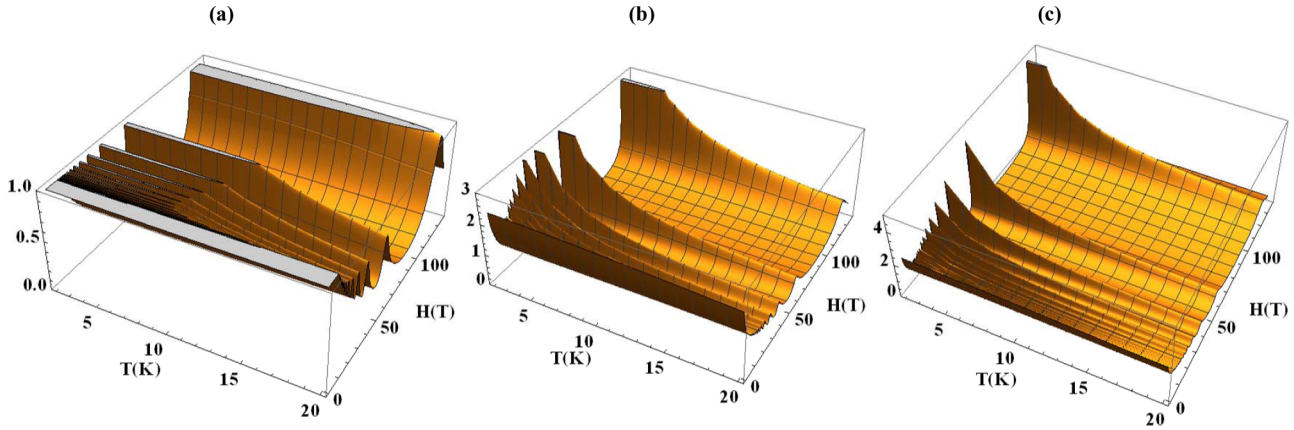

FIG. 3. The fragmented H-T phase diagram of the 2D Weyl semimetal. Cross sections (in gray) outline the superconducting domes. Three values of the effective electron-electron coupling are given. (a) $\lambda = 1$. (b) $\lambda = 0.33$. (c) $\lambda = 0.2$.

IV. GENERALIZATIONS: ZEEMAN COUPLING AND 3D WSMS

A. Zeeman coupling, the paramagnetic limit

Along with the orbital effect of the magnetic field on electrons and their pairing, at very high fields the direct (Zeeman) coupling of the magnetic field to spin becomes significant. A textbook example is the Chandrasekhar-Klogston [2] pair-breaking phenomenon in conventional metallic (parabolic single-band) superconductors.

To investigate the Zeeman coupling effect on superconductivity in (2D) WSMs, let us consider the following Hamiltonian:

$$H = K + K_Z + V. \tag{30}$$

Here the kinetic-energy term and the phonon-mediated effective interaction still are defined in Eqs. (1) and (2), respectively. The Zeeman coupling term is

$$K_Z = -g_L \mu_B H \int_{\mathbf{r}} \psi_\alpha^{s\dagger}(\mathbf{r}) \tau_{st}^z \delta_{\alpha\beta} \psi_\beta^t(\mathbf{r}), \tag{31}$$

where τ_{st}^z is the Pauli matrix in spin space and g_L and μ_B are the Lande factor and the Bohr magneton, respectively.

A simple singlet ansatz Eq. (4) no longer solves the set of the Gor'kov equations. Therefore they should be solved explicitly. The number of Green's functions in this case is doubled compared to the case considered in Sec. III. However the phase ansatz for the GF in the magnetic field Eq. (10) still holds. Substituting Eq. (10) into the gap equation [see Eq. (C3) of Appendix C where derivations also can be found] and using a pseudospin singlet ansatz for the gap function $\Delta_{\alpha\gamma}^*(\mathbf{r}) = \sigma_{\alpha\gamma}^x \exp(-r^2/2l^2)$, one obtains an equation for the critical curve on the H-T plane,

$$\frac{1}{\pi g^2} = T \sum_\omega \int_\rho \rho e^{-(\rho^2/2l^2)} \begin{pmatrix} g_{21}^{2\downarrow\downarrow}(-\boldsymbol{\rho}) g_{21}^{1\uparrow\uparrow}(\rho) + g_{22}^{2\uparrow\uparrow}(-\boldsymbol{\rho}) g_{11}^{1\downarrow\downarrow}(\rho) + g_{22}^{2\downarrow\downarrow}(-\boldsymbol{\rho}) g_{11}^{1\uparrow\uparrow}(\rho) + g_{21}^{2\uparrow\uparrow}(-\boldsymbol{\rho}) g_{21}^{1\downarrow\downarrow}(\rho) \\ g_{11}^{2\downarrow\downarrow}(-\boldsymbol{\rho}) g_{22}^{1\uparrow\uparrow}(\rho) + g_{11}^{2\uparrow\uparrow}(-\boldsymbol{\rho}) g_{22}^{1\downarrow\downarrow}(\rho) + g_{12}^{2\downarrow\downarrow}(-\rho) g_{12}^{1\uparrow\uparrow}(\rho) + g_{12}^{2\uparrow\uparrow}(-\boldsymbol{\rho}) g_{12}^{1\downarrow\downarrow}(\rho) \end{pmatrix}. \tag{32}$$

The set of spin-dependent GFs is calculated in Appendix C [Eqs. (C7) and (C8)].

Substituting them into Eq. (32), performing an integration over ρ and a summation on the Matsubara frequencies, one obtains a relation for the critical curve at the λ^{-1}-H plane,

$$\frac{1}{\lambda} = \frac{\overline{\omega}_c^2}{4\overline{\mu}} \sum_{n=0,m=0}^{\infty} \frac{(m+n)!}{2^{m+n}} \frac{f[n] f[m]}{m! n!} s_{nm}. \tag{33}$$

Here functions s_{nm} are as follows:

$$\begin{aligned} s_{nm} = {} & A_p\left[\overline{\omega}_c^2(n+1), \overline{\omega}_c^2(m+1), \overline{\mu}+\overline{\varepsilon}, \overline{\mu}-\overline{\varepsilon}\right] + A_p\left[\overline{\omega}_c^2(n+1), \overline{\omega}_c^2(m+1), \overline{\mu}-\overline{\varepsilon}, \overline{\mu}+\overline{\varepsilon}\right] + A_p\left[\overline{\omega}_c^2 n, \overline{\omega}_c^2 m, \overline{\mu}+\overline{\varepsilon}, \overline{\mu}-\overline{\varepsilon}\right] \\ & + A_p\left[\overline{\omega}_c^2 n, \overline{\omega}_c^2 m, \overline{\mu}-\overline{\varepsilon}, \overline{\mu}+\overline{\varepsilon}\right] + (\overline{\mu}^2 - \overline{\varepsilon}^2) \begin{pmatrix} B_p\left[\overline{\omega}_c^2(n+1), \overline{\omega}_c^2(m+1), \overline{\mu}+\overline{\varepsilon}, \overline{\mu}-\overline{\varepsilon}\right] \\ + B_p\left[\overline{\omega}_c^2(n+1), \overline{\omega}_c^2(m+1), \overline{\mu}-\overline{\varepsilon}, \overline{\mu}+\overline{\varepsilon}\right] \\ + B_p\left[\overline{\omega}_c^2 n, \overline{\omega}_c^2 m, \overline{\mu}+\overline{\varepsilon}, \overline{\mu}-\overline{\varepsilon}\right] + B_p\left[\overline{\omega}_c^2 n, \overline{\omega}_c^2 m, \overline{\mu}-\overline{\varepsilon}, \overline{\mu}+\overline{\varepsilon}\right] \end{pmatrix} \\ & + n\overline{\omega}_c^2 \left\{ B_p\left[\overline{\omega}_c^2(n+1), \overline{\omega}_c^2 m, \overline{\mu}+\overline{\varepsilon}, \overline{\mu}-\overline{\varepsilon}\right] + n B_p\left[\overline{\omega}_c^2(n+1), \overline{\omega}_c^2 m, \overline{\mu}-\overline{\varepsilon}, \overline{\mu}+\overline{\varepsilon}\right] \right\} \\ & + m B_p\left[\overline{\omega}_c^2 n, \overline{\omega}_c^2(m+1), \overline{\mu}+\overline{\varepsilon}, \overline{\mu}-\overline{\varepsilon}\right] + m B_p\left[\overline{\omega}_c^2 n, \overline{\omega}_c^2(m+1), \overline{\mu}-\overline{\varepsilon}, \overline{\mu}+\overline{\varepsilon}\right], \end{aligned} \tag{34}$$

where the dimensionless ratio of the Zeeman energy and temperature $\overline{\varepsilon} = 2 g_L \mu_B H / T$ is used. In the spin nondegenerate case the separation of the zero LL is not required due to the difference in chemical potentials of the spin projections. The Matsubara

sums read

$$A_p[a,b,\mu_1,\mu_2] = \frac{1}{4\sqrt{a}}\left\{\frac{(\sqrt{a}-\mu_1)^2\tanh\left[\frac{\sqrt{a}-\mu_1}{2}\right]}{(\sqrt{a}-\mu_1-\mu_2)^2-b} + \frac{(\sqrt{a}+\mu_1)^2\tanh\left[\frac{\sqrt{a}+\mu_1}{2}\right]}{(\sqrt{a}+\mu_1+\mu_2)^2-b}\right\} + \begin{pmatrix} a \longleftrightarrow b \\ \mu_1 \longleftrightarrow \mu_2 \end{pmatrix},$$

$$B_p[a,b,\mu_1,\mu_2] = \frac{1}{4\sqrt{a}}\left\{\frac{\tanh\left(\frac{\sqrt{a}-\mu_1}{2}\right)}{(\sqrt{a}-\mu_1-\mu_2)^2-b} + \frac{\tanh\left(\frac{\sqrt{a}+\mu_1}{2}\right)}{(\sqrt{a}+\mu_1+\mu_2)^2-b}\right\} - \begin{pmatrix} a \longleftrightarrow b \\ \mu_1 \longleftrightarrow \mu_2 \end{pmatrix}. \quad (35)$$

The results of the numerical calculations are presented in Fig. 4. The inverse effective coupling λ^{-1} as a function of the magnetic field for six values of the material parameter characterizing the strength of the Zeeman coupling on superconductivity $\alpha_p = g_L\mu_B c\Omega/ev^2$, $\alpha_p = 2\times10^{-4}$, 5×10^{-4},1.5×10^{-3},3.5×10^{-3},3.5×10^{-3},1.7×10^{-2} are plotted. The temperature is fixed at $T = 0.005\hbar\Omega$ (as above, we take $\hbar\Omega = 400$ K for concretions, and this amounts to 2 K), $\mu = 5\hbar\Omega$, whereas the range of magnetic fields is between $5\hbar c\Omega^2/ev^2$ and $30\hbar c\Omega^2/ev^2$. For a typical value of the Fermi velocity $c = 10^8$ cm/s this corresponds to 25–150 T. The magnetic phase (H-T) diagram is obtained as in the previous section as a set of fields for a fixed λ.

One observes that, whereas for the smallest Zeeman coupling (the blue curve) there is no difference with the zero Zeeman splitting case (the blue line in Fig. 2), for the largest value the superconductivity is quenched due to the Chandrasekhar-Klongstone (paramagnetic) limit. For the intermediate values of α_p the splitting of the superconducting domes of the fractured critical line is well pronounced.

Band-structure calculations of one of the most promising WSMs Cd_3As_2 show [19] that the Dirac point in this system is formed by the spin mixed with the sublattice index. In this case the Zeeman interaction with the external magnetic field is more complicated than considered in our two-band model. It is reasonable to expect however that qualitative features of the Zeeman coupling are similar. Another important characteristic of the superconducting WSM is that many of them are three dimensional.

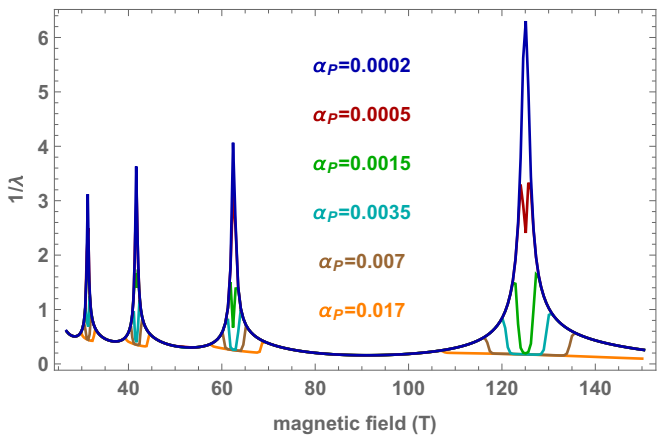

FIG. 4. Superconductor-normal critical curve on the λ^{-1}-H plane. Zeeman interaction splits the superconducting domes suppressing superconductivity at large values of the dimensionless paramagnetic coefficient $\alpha_p = g_L\mu_B c\Omega/ev^2$.

B. Generalization to a 3D WSM

In this subsection the calculation of the magnetic phase diagram is generalized to a 3D WSM with (typically several) Dirac points. The band structure of an asymmetric 3D WSM near such a point is captured by the Hamiltonian,

$$K = \int_{\mathbf{r}} \psi^{s\dagger}_{\alpha}(\mathbf{r},z)\{-i\hbar v(D_x\sigma^x_{\alpha\beta} + D_y\sigma^y_{\alpha\beta}) - i\hbar v_z\partial_z\sigma^z_{\alpha\beta} - \mu\delta_{\alpha\beta}\}\psi^s_{\beta}(\mathbf{r},z). \quad (36)$$

Here v is the Fermi velocity (assumed isotropic) on the x-y plane perpendicular to magnetic field, v_z is the Fermi velocity along the field, and the gauge in the covariant derivatives is chosen to be $\mathbf{A} = H(-y/2,x/2,0)$. The momentum p_z in this gauge is a conserved quantum number.

The calculation is analogous to the 2D one since the magnetic field enters the dependence Green's functions on lateral dimensions only. The Fourier transform is defined now by

$$G_{\gamma\kappa}(\mathbf{r},z,\tau) = T\sum_s \exp[-i\omega_s\tau + ip_z z]G_{\gamma\kappa}(\omega,\mathbf{r},p_z). \quad (37)$$

It is important to distinguish between the thin film and the "bulk" cases. For a film of thickness d, the field component of the momentum is discretized as

$$p_z = \frac{\pi\hbar}{d}M, \quad M = \pm1,2,\ldots. \quad (38)$$

The equations for two normal GFs [see Eqs. (7)] in the 3D case read

$$\begin{aligned}&[iv\mathbf{D}^i_r\cdot\sigma^i_{\gamma\beta} - v_z p_z\sigma^z_{\gamma\beta} + (i\omega+\mu)\delta_{\gamma\beta}]G^1_{\beta\kappa}(\mathbf{r},\mathbf{r}',p_z) = \delta^{\gamma\kappa}\delta(\mathbf{r}-\mathbf{r}'),\\ &[-iv\mathbf{D}^i_r\cdot\sigma^{ti}_{\gamma\beta} + v_z p_z\sigma^z_{\gamma\beta} + (-i\omega+\mu)\delta_{\gamma\beta}]G^2_{\beta\kappa}(\mathbf{r},\mathbf{r}',p_z) = \delta^{\gamma\kappa}\delta(\mathbf{r}-\mathbf{r}').\end{aligned} \quad (39)$$

The magnetic phase ansatz Eq. (10) still solves the 3D gap equation Eq. (7) (see Appendix D). Moreover the Gaussian form of the gap function (independent of z) Eq. (17) is not changed. The equation determining the critical curve on the H-T plane is now

$$\frac{1}{\lambda} = \frac{\zeta\overline{\omega}_c^2}{4\mu^2}\sum_{M>0}\left\{\sum_{n,m}\frac{(m+n)!}{2^{m+n+1}}\frac{f[n]f[m]}{m!n!}s_{nmM} + \sum_n\frac{f[n]f[0]}{2^n}s_{nM} + \frac{f[0]^2}{2}s_M\right\}. \quad (40)$$

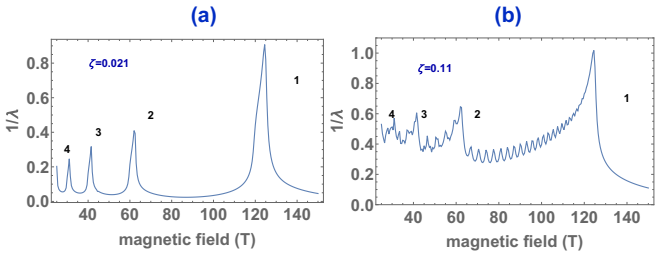

FIG. 5. Critical curve in the inverse coupling—magnetic-field (λ^{-1}-H) plane at a fixed temperature for the 3D WSM. The temperature value is $T = 0.005\hbar\Omega$. (a) Thick slab $\zeta \equiv \pi\hbar v_z/dT = 0.021$. (b) Thin film $\zeta = 0.11$. v_z is the electron velocity in the magnetic-field direction.

Here the 3D effective attraction strength (see Appendix D for the relevant DOS) is $\lambda = g^2\mu^2/2\pi^2 v_z v^2$, and the dimensionless parameter inversely proportional to the thickness is defined by $\zeta = \pi v_z/dT$. The functions s_{nmM}, s_{nM}, s_M depending on the new quantum number M, defined in Eq. (38) and details of derivation (including the relevant GF in this case) are given in Appendix D, whereas the function f containing the frequency dependence of the effective phonon-mediated interaction remains as in 2D, see Eq. (29).

The result for films of two values of the film thickness corresponding to values of $\zeta = 0.021$ and $\zeta = 0.11$ and fixed temperature $T = 0.005\hbar\Omega$ (for $\Omega = 400$ K it amounts to $T = 2$ K) are presented in Figs. 5(a) and 5(b), respectively. They demonstrate the essential transformation of the superconducting-normal fractured critical line compared to the 2D case. The smaller value of ζ practically corresponds to the bulk, whereas the larger value represents a thin film. In the bulk the domes become asymmetric due to the dispersion along the field. Generally larger coupling λ is required to create the superconducting state on the Landau levels. The phenomenon of the reentrant superconductivity itself however is clearly present due to enhancement of the DOS despite the fact that in 3D the DOS does not vanish between the LLs.

The superconducting domes become wider in slab geometry [Fig. 5(a)] and are demonstrated in a set of small secondary peaks (ripples) caused by the quantization of the momentum along the field (p_z) direction in a thin film. Higher LLs disappear. To conclude in the bulk the third dimension "smooths" the effect on Landau quantization as it appears in 2D but just slightly, whereas in thin films the shape is modified.

V. COMPARISON WITH EXPERIMENTS, DISCUSSION, AND CONCLUSIONS

In this section experimental evidence for the existence of the Cooper pairing in a WSM above H_{c2} is discussed. In addition we discuss the various tacit assumptions of our model and theoretical methods: Speculate on possible transition to a triplet superconducting phase and a necessity to go beyond the adiabatic approximation used in the present paper. The conventional metals are contrasted explicitly with Weyl semimetals.

A. Magnetoresistance as a signature of the superconducting state at Landau levels

A "smoking gun" revealing the existence of superconductivity on the Landau levels would be the dependence of resistivity on the magnetic field. In a normal metal one observes the resistivity generally increases faster than H superimposed with Shubnikov–de Haas (SdH) oscillations around the Landau levels. The picture is supported by detailed semiclassical theory valid for high Landau levels [20]. In the present paper the superconductivity in the quantum limit was studied. How will it influence the magnetoresistance at previously unreachable fields of order 100 T beyond the semiclassical regime?

Inside the superconducting domes (constituting a very tiny fraction of the magnetic phase diagram within the narrow range of fields) magnetoresistance does not vanish due to phenomenon of the "flux flow". Since 3D Weyl semimetals can be made very clean, an unpinned vortex liquid rather than a pinned vortex glass [21] is formed. When vortices are allowed to move, the dissipation inside the cores ensues, but the flux flow resistivity is much smaller than the normal state. In the vortex glass state the effect would be more dramatic: The resistivity drops (almost) to zero. It should be noted that vortices in the present context should be understood as an inhomogeneity of the order parameter since the magnetic "envelop" (of the size of the magnetic penetration depth) of multiple vortices strongly overlap at such fields. As a result magnetization is practically homogeneous [4,5]. Damping of the amplitude of the SdH oscillations in the superconducting regions is not expected to be significant as was noted already while analyzing the SdH oscillations in an organic superconductor [22] below the upper critical field of 3.6 T. The physics of the superconducting state on the LL in the quantum limit for the parabolic band material was theoretically described in a series of works [23].

In a remarkable experiment [9] with magnetic fields up to 50 T it was found that beyond several SdH oscillations at high LLs riding on magnetoresistance quadratic in H ($N = 6$–15 are clearly seen at $T = 3$ K) and upon approaching the quantum limit at $N = 2$–4 the magnetoresistance levels off. The amplitude of the oscillations gradually increases. It is very difficult to explain why the fast increase in the magnetoresistivity is halted at 10–20 T. It is natural to interpret this as the appearance of superconductivity as in Fig. 2 for moderate λ's. Indeed the superconductivity (in the dynamic vortex liquid flux flow phase) would strongly reduce the magnetoresistance magnitude. Our calculation is 2D, however the effect of 3D in a strong magnetic field is rather minor: The peaks in Figs. 2 and 3 will be broadened. In the experiment at $N = 2,3$ a significant Zeeman and pseudospin splitting (with and accompanying the Berry phase) are observed, and these will be discussed below. The splitting is seen clearly in the magnetoresistance data of Ref. [9] at fields above 25 T.

A similar phenomenon (less pronounced since the applied magnetic fields were up to 16 T only) was observed [24] in the Weyl superconductor TaP above H_{c2} while a quite conventional magnetic phase diagram was established experimentally below H_{c2}. (In this material $H_{c2}(1\text{ K}) = 3$ T and $T_c = 3.5$ K). As before, the fast increase in magnetoresistance

is leveled off at small N. Unfortunately it is difficult to assign definite N to SdH oscillations clearly seen at $T = 3$ K. This would correspond to the weak-coupling case shown in Figs. 2 and 3. The same relates to the recent discovery of the "logarithmic series" of oscillations [25] in the same material at a density on the order of 10^{16}. The quantum limit is reached, and the leveling of magnetoresistance is observed, but if superconductivity is formed at low Landau levels, it is nonadiabatic (see below).

B. On the possibility of the triplet pairing and type-II WSM

Our calculation was restricted to the singlet pairing. In some cases a strong magnetic field might in principle favor a triplet, however there is no experimental evidence in 3D Weyl semimetals for a triplet state so far. One therefore can ask the following question: Is the triplet state possible theoretically in models of the WSMs considered here. The question was addressed theoretically in a slightly different context of the 2D WSM surface state of a topological insulator [13,26]. In this system it was found that both the singlet and the triplet phases exist. However, although they are nearly degenerate in some cases (very small chemical potential μ), the singlet always prevails energetically. It also was shown theoretically [27] that magnetic impurities or proximity to the Stoner instability (local magnetic moment due to the exchange interaction) can favor the triplet state. In such a case the triplet superconducting state in the WSM must survive in extremely strong magnetic fields.

Another strong argument in 3D was put forward long ago by Rasolt and Tesanovic [5]. They argued that the Chandrasekhar-Klogston breaking of the singlet state is ineffective due to spacial inhomogeneity of the order parameter in the field direction. This remains valid for WSMs.

It was realized recently that this variety of novel Weyl materials should be differentiated [17,28,29] between the more isotropic "type-I" Weyl semimetals considered in the present paper and the highly anisotropic type-II Weyl semimetals in which the cone of the linear dispersion relation is tilted beyond a critical angle. The material becomes metallic with a very flat band. The critical temperature is higher, however one expects that the quantum limit is harder to achieve.

C. Comparison of the WSM superconductor to a conventional parabolic band superconductor adiabatic approximation

Let us complement the qualitative estimates made in the Introduction on the comparison between the pairing on Landau levels in the parabolic band materials (including semimetals [14]) and the WSM by contrasting the magnetic phase diagrams. Although the mechanism of pairing in WSM materials does not differ much from the conventional metals, the position of the superconducting domes does. Qualitatively the reason why the quantum limit is achievable at lower fields in this case is as follows. For a fixed chemical potential (near the band edge, that is, for values smaller than eV) the first Landau level in a Weyl semimetal appears at the field $c\mu^2/2e\hbar v^2$ compared to $cm^*\mu/e\hbar$ for the parabolic band. The ratio therefore is

$$\frac{H_{QL}^{\mathrm{WSM}}}{H_{QL}^{\mathrm{parabolic}}} = \frac{\mu}{2v^2m^*} \simeq \frac{\mu}{\mathrm{Ry}} \ll 1. \tag{41}$$

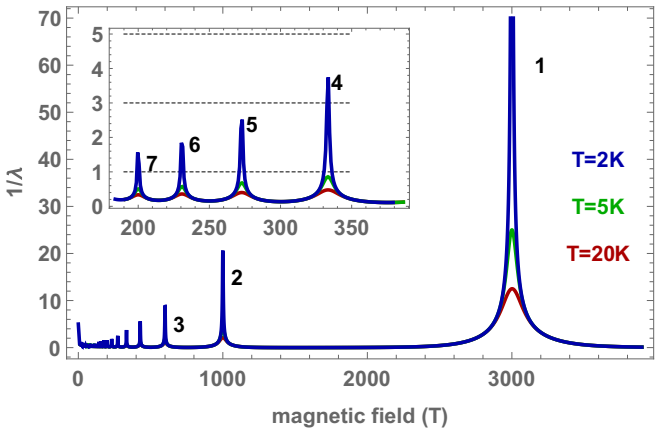

FIG. 6. The magnetic phase λ^{-1}-H for a conventional one-band metal.

Here the kinetic energy of the conventional parabolic band in metals was estimated as being on the order of Rydberg energy. This explains the small ratio of the estimate $H_{QL}^{WSM} = 100$ T, that favorably compares with the estimate for conventional parabolic band metals of at least an order of magnitude larger (see Fig. 6) where the phase diagram of the 2D single parabolic band superconductor with the electron-phonon coupling g, Debye frequency Ω, and the chemical potential $\mu = 5\hbar\Omega$ as for the WSMs in Sec. III (see the blue curve in Fig. 2) is presented. The effective mass of the conventional metal is assumed to be equal to that of the free-electron mass. The inverse effective coupling λ^{-1} (calculated with pertinent density of states) is given as a function of the magnetic field at the same temperatures $T = 0.005, 0.0125, 0.05\hbar\Omega$ (corresponding to 2, 5, and 20 K if $\hbar\Omega = 400$ K). The range of the magnetic field plotted is however much wider: 200–3000 T. The fields are necessarily superhigh if one were to attempt the quantum limit (low Landau level) for conventional metals as follows from the qualitative estimate in the Introduction. The inset shows (slightly) more accessible fields.

One observes that, although in the quantum limit the coupling required is not large, the fields are inaccessible. On the other hand, even beyond 100 T, one has superconducting domes at intermediate coupling at high LL $N \gg 10$ (so that the system enters the semiclassical regime [4] with weak quantization effects). The effect therefore is smeared out by disordering other effects. Note that, as demonstrated in Fig. 5, in 3D the peaks at higher LLs are broadened further and become unobservable.

Very recently superconductivity in a two-parabolic band semimetal in a strong magnetic field was considered [14]. One of the bands is quasiparticle with the distance of the band edge to the Fermi level $\mu_e \gg \hbar\Omega$ well within the adiabatic approximation, whereas the second is a hole with very small $\mu_h < \hbar\Omega$. The Landau quantization effect is most pronounced near the Lifshitz point where superconducting domes in the magnetic phase diagram clearly are seen.

It is important to note that assumptions of our calculation include the adiabatic pairing, namely, that the Fermi level is larger than the Debye energy $\mu/\Omega > 1$. WSM-like $ZrTe_5$ also can be tuned to a small chemical potential [30], however

to make use of the Gaussian approximation (in the BCS form or the Eliashberg form), one typically relies on the Migdal theorem [16]. Here it is questionable [12]. Therefore in the present paper only the adiabatic case of $\mu/\hbar\Omega > 5$ was discussed. It would be interesting to investigate what will happen beyond this assumption since in many Dirac materials the Fermi energy is very low. For example, in the Fermi energy in $ZrTe_5$ grown in Ref. [30] in experiment in large fields up to 100 T no oscillations were observed at all. However in this experiment the density is below 10^{15} cm^{-3}.

VI. CONCLUSIONS

In this paper, the microscopic theory of phonon-mediated superconductivity in (type-I) Weyl semimetals at very high magnetic fields was constructed. Although weak coupling was assumed, the retardation effects were taken into account. It was shown that a Weyl semimetal in 2D and 3D that is nonsuperconducting or having a low critical temperature T_c at zero field becomes superconducting in narrow regions of the magnetic phase diagram around the Landau levels especially near the quantum limit. The Zeeman splitting sometimes becomes of significance at the highest fields. Superconductivity has an effect on magnetoconductivity beyond the conventional H_{c2}. Near the Landau levels the magnetoresistivity should diminish. This might explain the recent experiments on Cd_3As_2 and TaP and perhaps other semimetals.

This enhancement especially is pronounced for the lowest Landau level. As a consequence, the reentrant superconducting regions in the temperature-field phase diagram emerge at low temperatures near the magnetic fields at which the chemical potential matches the Landau levels.

ACKNOWLEDGMENTS

We are grateful to N. L. Wang, T. Maniv, T. W. Luo, V. Vinokur, J. Wang, and C. Hou, for valuable discussions. B.R. acknowledges MOST of ROC Grant No. 103-2112-M-009-009-MY3 hospitality of Peking and Bar Ilan Universities. D.P.L. was supported by the National Natural Science Foundation of China (Grants No. 11274018 and No. 11674007).

APPENDIX A: CALCULATION OF THE NORMAL GREEN'S FUNCTIONS

In this Appendix the normal-state Green's functions are calculated. In the matrix form Eqs. (11) and (12) read

$$\widehat{h}^a g^a(\rho) = \delta(\rho), \tag{A1}$$

with 2D matrix operators $\widehat{h}^1 = i\omega + \mu - \Pi\cdot\sigma$, $\widehat{h}^2 = -i\omega + \mu + \Pi\cdot\sigma^t$, where $a = 1,2$ and $\Pi = \{\Pi_x,\Pi_y\}$ are the ladder operators. In the symmetric gauge,

$$\Pi_x = -i\frac{\partial}{\partial\rho_x} + \frac{1}{2l^2}\rho_y, \quad \Pi_y = -i\frac{\partial}{\partial\rho_y} - \frac{1}{2l^2}\rho_x. \tag{A2}$$

It is convenient to rewrite them via creation and annihilation operators for a bosonic field,

$$a = \frac{l}{\sqrt{2}}(\Pi_x - i\Pi_y), \quad a^\dagger = \frac{l}{\sqrt{2}}(\Pi_x + i\Pi_y), \tag{A3}$$

with the commutation relations $[\Pi_x,\Pi_y] = -i/l^2$, $[a,a^\dagger] = 1$.

The matrix elements of the 2×2 matrices h^a are defined by relations,

$$h^1_{11} = h^1_{22} = i\omega + \mu, \quad h^2_{11} = h^2_{22} = -i\omega + \mu,$$
$$\widehat{h}^1_{12} = \widehat{h}^2_{21} = -\omega_c a, \quad \widehat{h}^1_{21} = \widehat{h}^2_{12} = -\omega_c a^\dagger. \tag{A4}$$

Here $\omega_c = v\sqrt{2}/l$ is the Larmor frequency in the Weyl semimetals. Equations for normal GFs can be represented in the following form (suppressing the index a):

$$h_{11}g_{11} + \widehat{h}_{12}g_{21} = \delta(\rho), \quad \widehat{h}_{21}g_{12} + h_{22}g_{22} = \delta(\rho),$$
$$h_{11}g_{12} + \widehat{h}_{12}g_{22} = 0, \quad \widehat{h}_{21}g_{11} + h_{22}g_{21} = 0. \tag{A5}$$

Since h_{11},h_{22} are just numbers (not operators acting on ρ), one first solves the second pair of equations for the off-diagonal elements,

$$g_{21} = -\frac{1}{h_{22}}\widehat{h}_{21}g_{11}, \quad g_{12} = -\frac{1}{h_{11}}\widehat{h}_{12}g_{22}. \tag{A6}$$

Substituting into the first pair, one obtains

$$(h_{22}h_{11} - \widehat{h}_{12}\widehat{h}_{21})g_{11}(\rho) = h_{22}\delta(\rho), \tag{A7}$$

$$(h_{11}h_{22} - \widehat{h}_{21}\widehat{h}_{12})g_{22}(\rho) = h_{11}\delta(\rho). \tag{A8}$$

We present next a detailed calculation of the normal GF, whereas the associate GFs are obtained similarly. For g^1_{11}, after substitution of the matrix elements from Eq. (A4), one obtains the following second-order linear differential equation with a source:

$$\{(i\omega+\mu)^2 - \Pi^2 - i[\Pi_x,\Pi_y]\}g^1_{11}(\rho) = (i\omega+\mu)\delta(\rho). \tag{A9}$$

This is written via the Laplacian,

$$\widehat{L} = \frac{l^2}{2}\left\{-\frac{\partial^2}{\partial\rho^2} - \frac{1}{\rho}\frac{\partial}{\partial\rho} - \frac{1}{\rho^2}\frac{\partial^2}{\partial\theta^2} + \frac{i}{2l^2}\frac{\partial}{\partial\theta} + \frac{\rho^2}{4l^4}\right\}, \tag{A10}$$

as represented into the form

$$\left((i\omega+\mu)^2 - \frac{\omega_c^2}{2} - \omega_c^2\widehat{L}\right)g^1_{11}(\rho) = (i\omega+\mu)\delta(\rho). \tag{A11}$$

Since the operator $\widehat{L}$ in this equation is rotation invariant, $g^1_{11}(\rho)$ is a scalar (independent of the polar angle). The operator $\widehat{L}$ has the following eigenfunctions and eigenvalues [31]:

$$\epsilon^m_n = n + \frac{|m| + m + 1}{2}, \tag{A12}$$

and eigenfunctions,

$$\varphi^m_n = \frac{1}{l^{1+|m|}}\sqrt{\frac{n!}{2^{|m|}(|m|+n)!}}\exp\left[-\frac{\rho^2}{4l^2}\right]$$
$$\times\,\rho^{|m|}L^{|m|}_n\left(\frac{\rho^2}{2l^2}\right)\frac{e^{im\theta}}{\sqrt{2\pi}}. \tag{A13}$$

Here n and m are integers, and L^m_n's are the generalized Laguerre polynomials.

In the specific case of a scalar, the azimuthal number is $m = 0$, and one obtains

$$\varphi_n^0 = \frac{1}{\sqrt{2\pi}l}\exp\left[-\frac{\rho^2}{4l^2}\right]L_n\left[\frac{\rho^2}{2l^2}\right]. \tag{A14}$$

Expanding the GF $g_{11}^1(\rho)$ by a series of the scalar eigenfunctions of the $\widehat{L}$ operator $g_{11}^1(\rho) = \sum_n c_n^0\varphi_n^0$ and making the scalar product with φ_n^0, one obtains

$$\int_\rho \varphi_{n'}^{0*}\sum_{nm}\left[(i\omega+\mu)^2 - \omega_c^2(1+n)\right]c_n^0\varphi_n^0 = (i\omega+\mu)\int_\rho \varphi_{n'}^{0*}(\rho)\delta(\rho). \tag{A15}$$

Performing the integration, finally,

$$g_{11}^1(\rho) = \frac{i\omega+\mu}{2\pi l^2}\exp[-\rho^2/4l^2] \times \sum_{n=0}\frac{L_n[\rho^2/2l^2]}{(i\omega+\mu)^2 - \omega_c^2(1+n)}. \tag{A16}$$

Using the relation Eq. (A6), the off-diagonal matrix element $g_{21}^1(\rho)$ reads

$$g_{21}^1(\rho) = \frac{\omega_c}{i\omega+\mu}a^\dagger g_{11}^1(\rho). \tag{A17}$$

Since

$$a^\dagger = \frac{i}{\omega_c}e^{i\theta}\left(\frac{\partial}{\partial\rho} - \frac{i}{\rho}\frac{\partial}{\partial\theta} + \frac{\rho}{2l^2}\right), \tag{A18}$$

using the relation between Laguerre polynomials [18], the result is as follows:

$$g_{21}^1(\rho) = \frac{i\rho}{2\pi l^4}e^{i\theta}\exp[-\rho^2/4l^2]\sum_{n=1}\frac{L_{n-1}^1[\rho^2/2l^2]}{(i\omega+\mu)^2 - \omega_c^2(1+n)}. \tag{A19}$$

In order to calculate the next pair of GF matrix elements g_{22}^1 and g_{12}^1, one has to solve the second Eq. (A7). The corresponding equation is similar

$$\left[-\omega_c^2 a^\dagger a + (i\omega+\mu)^2\right]g_{22}^1(\rho) = (i\omega+\mu)\delta(\rho), \tag{A20}$$

$$\left\{(i\omega+\mu)^2 - \omega_c^2\widehat{L}\right\}g_{22}^1(\rho) = (i\omega+\mu)\delta(\rho). \tag{A21}$$

Repeating the procedure this results in

$$g_{22}^1(\rho) = \frac{i\omega+\mu}{2\pi l^2}\exp[-\rho^2/4l^2]\sum_{n=0}\frac{L_n[\rho^2/2l^2]}{(i\omega+\mu)^2 - \omega_c^2 n}. \tag{A22}$$

Using the relation $g_{12}^1(\rho) = \frac{\omega_c}{i\omega+\mu}a g_{22}^1(\rho)$, one obtains in view of

$$a = -\frac{ie^{-i\theta}}{\omega_c}\left(-\frac{\partial}{\partial\rho} - \frac{i}{\rho}\frac{\partial}{\partial\theta} + \frac{\rho}{2l^2}\right),$$

$$g_{12}^1(\rho) = i\frac{ve^{-i\theta}}{2\pi l^4}\rho\exp\left[-\frac{\rho^2}{4l^2}\right]\sum_{n=1}\frac{L_n^1[\rho^2/2l^2]}{(i\omega+\mu)^2 - \omega_c^2 n}. \tag{A23}$$

The associated GF is calculated in the same manner replacing matrix elements as is presented in Eq. (A4). All of the GFs are presented in Eqs. (14) and (15).

APPENDIX B: MATSUBARA SUMMATIONS

The sums over reduced Matsubara frequency $\overline{\omega}_s = \pi(2s+1)$ in Eq. (22) read

$$A_1[a,b] = \sum_{s=-\infty}^{\infty}\frac{\overline{\omega}_s^2 + \overline{\mu}^2}{\left[(-i\overline{\omega}_s+\overline{\mu})^2 - \overline{\omega}_c^2(n+1)\right]\left[(i\overline{\omega}_s+\mu)^2 - \overline{\omega}_c^2(m+1)\right]} = \frac{(\sqrt{a}-\mu)^2\tanh\left(\frac{\sqrt{a}-\mu}{2}\right)}{4\sqrt{a}[-b+(\sqrt{a}-2\mu)^2]} + \frac{(\sqrt{b}-\mu)^2\tanh\left(\frac{\sqrt{b}-\mu}{2}\right)}{4\sqrt{b}[-a+(\sqrt{b}-2\mu)^2]}, \tag{B1}$$

$$A_2[a,b] = \sum_s\frac{\overline{\omega}_s^2 + \overline{\mu}^2}{\left[(-i\overline{\omega}_s+\overline{\mu})^2 - \overline{\omega}_c^2 n\right]\left[(i\overline{\omega}_s+\overline{\mu})^2 - \overline{\omega}_c^2 m\right]} = \frac{(\sqrt{a}+\mu)^2\tanh\left(\frac{\sqrt{a}+\mu}{2}\right)}{4\sqrt{a}[-b+(\sqrt{a}+2\mu)^2]} + \frac{(\sqrt{b}+\mu)^2\tanh\left(\frac{\sqrt{b}+\mu}{2}\right)}{4\sqrt{b}[-a+(\sqrt{b}+2\mu)^2]}, \tag{B2}$$

$$B_1[a,b] = \sum_s\frac{n}{\left[(-i\overline{\omega}_s+\overline{\mu})^2 - \overline{\omega}_s^2(n+1)\right]\left\{\left[(i\overline{\omega}_s+\overline{\mu})^2 - \overline{\omega}_c^2 m\right]\right\}} = -\frac{\tanh\left(\frac{\sqrt{a}-\overline{\mu}}{2}\right)}{4\sqrt{a}[-b+(\sqrt{a}-2\overline{\mu})^2]} - \frac{\tanh\left(\frac{\sqrt{b}-\overline{\mu}}{2}\right)}{4\sqrt{b}[-a+(\sqrt{b}-2\overline{\mu})^2]}, \tag{B3}$$

and

$$B_2[a,b] = \sum_s\frac{m}{\left[(-i\overline{\omega}_s+\overline{\mu})^2 - \overline{\omega}_c^2 n\right]\left[(i\overline{\omega}_s+\overline{\mu})^2 - \overline{\omega}_c^2(m+1)\right]} = -\frac{\tanh\left[\frac{\sqrt{a}+\overline{\mu}}{2}\right]}{4\sqrt{a}[-b+(\sqrt{a}+2\overline{\mu})^2]} - \frac{\tanh\left[\frac{\sqrt{b}+\overline{\mu}}{2}\right]}{4\sqrt{b}[-a+(\sqrt{b}+2\overline{\mu})^2]}. \tag{B4}$$

Functions $A[a,b]$ and $B[a,b]$ in Eq. (24) are composed subsequently as

$$A[a,b] = A_1[a,b] + A_2[a,b], \quad B[a,b] = B_1[a,b] + B_2[a,b]. \tag{B5}$$

APPENDIX C: THE ZEEMAN EFFECT

1. The Zeeman term in Gor'kov equations

In the case of the WSM Hamiltonian containing the Zeeman term Eq. (30), the Gor'kov equations for the normal Green's function at criticality reads

$$\frac{\partial G^{st}_{\gamma\kappa}(X,X')}{\partial\tau} = i\sigma^i_{\gamma\beta}\partial_r G^{st}_{\beta\kappa}(X,X') + \mu G^{st}_{\gamma\kappa}(X,X') + g_L\mu_B H\tau^z_{st'}G^{t't}_{\gamma\kappa}(X,X') - \delta^{\gamma\kappa}\delta^{ts}\delta(X-X'), \tag{C1}$$

whereas the equation for the anomalous average becomes

$$\frac{\partial F^{st+}_{\gamma\kappa}(X,X')}{\partial\tau} = iv\sigma^i_{\alpha\gamma}\nabla^i_r F^{st+}_{\alpha\kappa}(X,X') - \mu F^{+st}_{\gamma\kappa}(X,X') - \frac{g^2}{4}\varepsilon^{s_1s_2}F^{+s_1s_2}_{\alpha\gamma}(X,X)\varepsilon^{s_3s}G^{s_3t}_{\alpha\kappa} - g_L\mu_B H\tau^z_{st'}F^{t't+}_{\gamma\kappa}(X,X'). \tag{C2}$$

The number of GFs in this case is doubled, although due to symmetry for the singlet pairing solution one observes that $G^{\uparrow\downarrow}_{\gamma\kappa} = G^{\downarrow\uparrow}_{\gamma\kappa} = F^{+\uparrow\uparrow}_{\gamma\kappa} = F^{+\downarrow\downarrow}_{\gamma\kappa} = 0$.

The self-consistent equation for the gap function is as follows:

$$\Delta^*_{\beta\kappa}(\mathbf{r}) = -\frac{g^2}{4}\int_{\mathbf{r}'}\left[G^{2\downarrow\downarrow}_{\beta\gamma}(\mathbf{r}',\mathbf{r})\Delta^*_{\alpha\gamma}(\mathbf{r}')G^{1\uparrow\uparrow}_{\alpha\kappa}(\mathbf{r},\mathbf{r}') + G^{2\uparrow\uparrow+}_{\beta\gamma}(\mathbf{r}',\mathbf{r})\Delta^*_{\alpha\gamma}(\mathbf{r}')G^{1\downarrow\downarrow}_{\alpha\kappa}(\mathbf{r},\mathbf{r}')\right], \tag{C3}$$

whereas the GFs in the magnetic field are

$$\begin{aligned} G^{ss1}_{\beta\kappa}(\mathbf{r},\mathbf{r}') &= \exp\left[-i\frac{xy'-yx'}{2l^2}\right]g^{ss1}_{\beta\kappa}(\mathbf{r}-\mathbf{r}'),\\ G^{ss2}_{\beta\kappa}(\mathbf{r}',\mathbf{r}) &= \exp\left[-i\frac{xy'-yx'}{2l^2}\right]g^{ss2}_{\beta\kappa}(\mathbf{r}'-\mathbf{r}), \end{aligned} \tag{C4}$$

here $s = \uparrow,\downarrow$.

Substituting Eq. (C4) into Eq. (C3) and using the singlet assumption $\Delta^*_{\alpha\gamma}(\mathbf{r}) = \Delta(\mathbf{r})\sigma^x_{\alpha\gamma}$, one obtains Eq. (18) and after the angle integration Eq. (20) with the only difference being the modified function S,

$$S_Z(\rho,\omega) = \begin{pmatrix} g^{2\downarrow\downarrow}_{21}(-\rho)g^{1\uparrow\uparrow}_{21}(\rho) + g^{2\uparrow\uparrow}_{22}(-\rho)g^{1\downarrow\downarrow}_{11}(\rho) + g^{2\downarrow\downarrow}_{22}(-\rho)g^{1\uparrow\uparrow}_{11}(\rho) + g^{2\uparrow\uparrow}_{21}(-\rho)g^{1\downarrow\downarrow}_{21}(\rho) \\ g^{2\downarrow\downarrow}_{11}(-\rho)g^{1\uparrow\uparrow}_{22}(\rho) + g^{2\uparrow\uparrow}_{11}(-\rho)g^{1\downarrow\downarrow}_{22}(\rho) + g^{2\downarrow\downarrow}_{12}(-\rho)g^{1\uparrow\uparrow}_{12}(\rho) + g^{2\uparrow\uparrow}_{12}(-\rho)g^{1\downarrow\downarrow}_{12}(\rho) \end{pmatrix}. \tag{C5}$$

2. Calculation of the GF

Calculation of the GF is performed along the lines described in Appendix A. In this case however we get two separate equations for each GF with different spin projections. The equations for the first GF are as follows:

$$\begin{aligned} i\omega G^{1\uparrow\uparrow}_{\gamma\kappa}(\mathbf{r},\mathbf{r}') - i\sigma^i_{\gamma\beta}\partial_r G^{1\uparrow\uparrow}_{\beta\kappa}(\mathbf{r},\mathbf{r}') + (\mu + g_L\mu_B H)G^{1\uparrow\uparrow}_{\gamma\kappa}(\mathbf{r},\mathbf{r}') &= \delta^{\gamma\kappa}\delta(\mathbf{r}-\mathbf{r}'),\\ i\omega G^{1\downarrow\downarrow}_{\gamma\kappa}(\mathbf{r},\mathbf{r}') - i\sigma^i_{\gamma\beta}\partial_r G^{1\downarrow\downarrow}_{\beta\kappa}(\mathbf{r},\mathbf{r}') + (\mu - g_L\mu_B H)G^{1\downarrow\downarrow}_{\gamma\kappa}(\mathbf{r},\mathbf{r}') &= \delta^{\gamma\kappa}\delta(\mathbf{r}-\mathbf{r}'). \end{aligned} \tag{C6}$$

Therefore the solution coincides with that of the GF Eq. (14) for two different values of the chemical potential. The result is

$$\begin{aligned} g^{1\uparrow\uparrow,\downarrow\downarrow}_{11}(\rho) &= \frac{(i\omega+\mu\pm g_L\mu_B H)}{2\pi l^2}\exp\left[-\frac{\rho^2}{4l^2}\right]\sum_{n=0}\frac{L_n[\rho^2/2l^2]}{(i\omega+\mu\pm g_L\mu_B H)^2-\omega_c^2(1+n)},\\ g^{1\uparrow\uparrow,\downarrow\downarrow}_{21}(\rho) &= \frac{iv\rho e^{i\theta}}{2\pi l^4}\exp\left[-\frac{\rho^2}{4l^2}\right]\sum_{n=1}\frac{L^1_{n-1}[\rho^2/2l^2]}{(i\omega+\mu\pm g_L\mu_B H)^2-\omega_c^2(1+n)},w\\ g^{1\uparrow\uparrow,\downarrow\downarrow}_{22}(\rho) &= \frac{(i\omega+\mu\pm g_L\mu_B H)}{2\pi l^2}\exp\left[-\frac{\rho^2}{4l^2}\right]\sum_{n=0}\frac{L_n[\rho^2/2l^2]}{(i\omega+\mu\pm g_L\mu_B H)^2-\omega_c^2 n},\\ g^{1\uparrow\uparrow,\downarrow\downarrow}_{12}(\rho) &= \frac{iv\rho e^{-i\theta}}{2\pi l^4}\exp\left[-\frac{\rho^2}{4l^2}\right]\sum_{n=1}\frac{L^1_n[\rho^2/2l^2]}{\left[t(i\omega+\mu\pm\mu_Z H)^2-\omega_c^2 n\right]}. \end{aligned} \tag{C7}$$

Similarly for the second set of GFs,

$$g_{11}^{2\uparrow\uparrow,\downarrow\downarrow}(-\rho)=\frac{(-i\omega+\mu\pm g_L\mu_B H)}{2\pi l^2}\exp\left[-\frac{\rho^2}{4l^2}\right]\sum_{n=0}\frac{L_n[\rho^2/2l^2]}{(-i\omega+\mu\pm g_L\mu_B H)^2-\omega_c^2 n},$$

$$g_{12}^{2\uparrow\uparrow,\downarrow\downarrow}(-\rho)=\frac{iv\rho e^{i\theta}}{2\pi l^4}\exp\left[-\frac{\rho^2}{4l^2}\right]\sum_{n=1}^{\infty}\frac{L_{n-1}^1[\rho^2/2l^2]}{(-i\omega+\mu\pm g_L\mu_B H)^2-\omega_c^2(n+1)},$$

$$g_{21}^{2\uparrow\uparrow,\downarrow\downarrow}(-\rho)=-\frac{iv\rho e^{-i\theta}}{2\pi l^4}\exp\left[-\frac{\rho^2}{4l^2}\right]\sum_{n=1}^{\infty}\frac{L_n^1[\rho^2/2l^2]}{(-i\omega+\mu\pm g_L\mu_B H)^2-\omega_c^2 n},$$

$$g_{22}^{2\uparrow\uparrow,\downarrow\downarrow}(-\rho)=\frac{(-i\omega+\mu\pm g_L\mu_B H)}{2\pi l^2}\exp\left[-\frac{\rho^2}{4l^2}\right]\sum_{n=0}^{\infty}\frac{L_n[\rho^2/2l^2]}{(-i\omega+\mu\pm g_L\mu_B H)^2-\omega_c^2(n+1)} \tag{C8}$$

APPENDIX D: GENERALIZATION TO 3D

1. Density of states for a film in a zero magnetic field

Using the dispersion law in the form

$$\varepsilon=\sqrt{v^2\left(p_x^2+p_y^2\right)+v_z^2p_z^2}, \tag{D1}$$

one obtains for the density of electrons for the bulk anisotropic sample,

$$n=\frac{1}{(2\pi)^3\hbar^3}\int_p\Theta(\varepsilon[p]-\mu)=\frac{\mu^3}{6\pi^2v_zc_x^2\hbar^3}, \tag{D2}$$

whereas the density of electron states,

$$D(\mu)=\frac{\mu^2}{2\pi^2v_zv^2\hbar^3}. \tag{D3}$$

In films of thickness d the quantization of the momentum along axes z is important, and the density of the electrons reads

$$n[\mu]=\frac{N}{Ad}=\frac{1}{(2\pi)^2\hbar^2}\frac{1}{2d}\int_{\mathbf{p}}\sum_M\Theta(\varepsilon[\mathbf{p},M]-\mu), \tag{D4}$$

where $\varepsilon^2[p,M]=v^2(p_x^2+p_y^2)+v_z^2(\pi\hbar M/d)^2=v^2p^2+v_z^2(\pi\hbar M/d)^2$ and the chemical potential is $\mu=\sqrt{v^2u+v_z^2(\pi\hbar M/d)^2}$. The density of states in this case is

$$D(\mu)=\frac{dn}{d\mu}=\frac{1}{8\pi\hbar^2d}\sum_{M:\mu>\mu_M}\frac{2\mu}{v^2}=\frac{\mu}{4\pi\hbar^2dv^2}F[\mu]. \tag{D5}$$

Here $\mu_M=\frac{\pi\hbar}{d}v_z|M|$ with $M[\mu]=\frac{d}{\pi\hbar v_z}\mu_M$, while $F[\mu]$ is the step-like function: $F=2n$ in the interval $\frac{\pi\hbar}{d}v_zn\pi<\mu<(n+1)\frac{\pi\hbar}{d}v_z\pi$, $n=1,2,3\ldots$.

2. Green's functions in 3D

In this Appendix the normal-state Green's functions for 3D are calculated. In the matrix form Eqs. (11) and (12) read

$$\widehat{h}^a g^a(\rho)=\delta(\rho), \tag{D6}$$

where $a=1,2$ with 3D matrix operators,

$$\widehat{h}^1=i\omega+\mu-\Pi\cdot\sigma-v_zp_z\sigma^z,\quad \widehat{h}^2=-i\omega+\mu+\Pi\cdot\sigma^t+v_zp_z\sigma^z. \tag{D7}$$

Substituting $\widehat{h}^1$ and $\widehat{h}^2$ into Eq. (C6) and solving the set of eight equations in the manner similar to that described in Appendix A, one obtains the first set of GFs,

$$g_{11}^1(\rho,p_z)=\frac{v_zp_z+i\omega+\mu}{2\pi l^2}\exp\left[-\frac{\rho^2}{4l^2}\right]\sum_{n=0}\frac{L_n[\rho^2/2l^2]}{(i\omega+\mu)^2-v_z^2p_z^2-\omega_c^2(n+1)},$$

$$g_{12}^1(\rho,p_z)=-\frac{i\rho e^{-i\theta}}{2\pi l^4}\exp\left[-\frac{\rho^2}{4l^2}\right]\sum_{n=1}\frac{L_n^1[\rho^2/2l^2]}{(i\omega+\mu)^2-v_z^2p_z^2-\omega_c^2n},$$

$$g^1_{22}(\rho,p_z)=\frac{-v_zp_z+i\omega+\mu}{2\pi l^2}\exp\left[-\frac{\rho^2}{4l^2}\right]\sum_{n=0}\frac{L_n[\rho^2/2l^2]}{(i\omega+\mu)^2-v_z^2p_z^2-\omega_c^2n},$$
$$g^1_{21}(\rho,p_z)=-\frac{ie^{i\theta}\rho}{2\pi l^4}\exp\left[-\frac{\rho^2}{4l^2}\right]\sum_{n=1}\frac{L^1_{n-1}[\rho^2/2l^2]}{(i\omega+\mu)^2-v_z^2p_z^2-\omega_c^2(n+1)}, \tag{D8}$$

and the second set,

$$g^2_{11}(-\rho,-p_z)=\frac{-v_zp_z+i\omega+\mu}{2\pi l^2}\exp\left[-\frac{\rho^2}{4l^2}\right]\sum_{n=0}\frac{L_n[\rho^2/2l^2]}{(i\omega+\mu)^2-v_z^2p_z^2-\omega_c^2(1+n)},$$
$$g^2_{12}(-\rho,-p_z)=\frac{ie^{i\theta}\rho}{2\pi l^4}\exp\left[-\frac{\rho^2}{4l^2}\right]\sum_{n=1}\frac{L^1_n[\rho^2/2l^2]}{(i\omega+\mu)^2-v_z^2p_z^2-\omega_c^2n},$$
$$g^2_{22}(-\rho,-p_z)=\frac{v_zp_z+i\omega+\mu}{2\pi l^2}\exp\left[-\frac{\rho^2}{4l^2}\right]\sum_{n=0}\frac{L_n[\rho^2/2l^2]}{(i\omega+\mu)^2-v_z^2p_z^2-\omega_c^2n}, \tag{D9}$$
$$g^2_{21}(-\rho,-p_z)=\frac{ie^{-i\theta}\rho}{2\pi l^4}\exp\left[-\frac{\rho^2}{4l^2}\right]\sum_{n=1}\frac{L^1_{n-1}[\rho^2/2l^2]}{(i\omega+\mu)^2-v_z^2p_z^2-\omega_c^2(1+n)}.$$

These functions allow for solving exactly the gap equation.

3. Solution of the gap equation in 3D

The gap equation in 3D takes the form

$$\Delta(\mathbf{r})=\frac{g^2T}{2}\sum_\omega\int_{\mathbf{r}'}\exp\left[-i\frac{xy'-yx'}{l^2}\right]\Delta^*(\mathbf{r}')\left[\begin{array}{l}g^2_{22}(-\rho,-p_z)g^1_{11}(\rho,p_z)+g^2_{11}(-\rho,-p_z)g^1_{22}(\rho,p_z)\\+g^2_{12}(-\rho,-p_z)g^1_{12}(\rho,p_z)+g^2_{21}(-\rho,-p_z)g^1_{21}(\rho,p_z)\end{array}\right], \tag{D10}$$

where $\rho=\mathbf{r}-\mathbf{r}'$,$\mathbf{r}$,$\mathbf{r}'$ are vectors on the x-y plane. Substituting the ansatz for the gap function Eq. (17) and GF Eqs. (D8) and (D9) into Eq. (D10) and performing integration over the angle as in the 2D case, one obtains the equation (using the notation $u=\rho^2/2l^2$),

$$\frac{2}{g^2}=\frac{1}{2\pi l^2}\sum_{\omega,p_z}\int_u e^{-2u}S(u,p_z,\omega). \tag{D11}$$

Here,

$$\begin{aligned}S(u,p_z,\omega)=&\sum_{n,m=0}\left\{\frac{[\omega^2+(\mu-v_zp_z)^2]L_n[u]L_m[u]}{[(-i\omega+\mu)^2-v_z^2p_z^2-\omega_c^2(n+1)][(i\omega+\mu)^2-v_z^2p_z^2-\omega_c^2(m+1)]}\right.\\&\left.+\frac{[\omega^2+(\mu+v_zp_z)^2]L_n[u]L_m[u]}{[(-i\omega+\mu)^2-v_z^2p_z^2-\omega_c^2n][(i\omega+\mu)^2-v_z^2p_z^2-\omega_c^2m]}\right\}\\&+\sum_{n,m=1}\left\{\frac{\omega_c^2uL^1_{n-1}[u]L^1_m[u]}{[(-i\omega+\mu)^2-v_z^2p_z^2-\omega_c^2(n+1)][(i\omega+\mu)^2-v_z^2p_z^2-\omega_c^2m]}\right.\\&\left.+\frac{\omega_c^2uL^1_n[u]L^1_{m-1}[u]}{[(-i\omega+\mu)^2-v_z^2p_z^2-\omega_c^2n][(i\omega+\mu)^2-v_z^2p_z^2-\omega_c^2(m+1)]}\right\}.\end{aligned} \tag{D12}$$

After integration over u it is written as a double sum,

$$\frac{1}{\lambda}=\frac{\zeta\overline{\omega}_c^2}{4\mu^2}\sum_{s,M}\left\{\sum_{n,m=1,s}\frac{(m+n)!f[n]f[m]}{2^{m+n+1}m!n!}S_1+\sum_{n=1,s}\frac{f[n]f[0]}{2^n}S_2+\frac{f[0]^2}{2}\sum_sS_3\right\}, \tag{D13}$$

where

$$\begin{aligned}S_1=&\frac{\omega_s^2+\mu^2+(\zeta M)^2}{[(-i\omega_s+\mu)^2-(\zeta M)^2-\omega_c^2(n+1)][(i\omega_s+\mu)^2(\zeta M)^2-\omega_c^2(m+1)]}\\&+\frac{\omega_s^2+\mu^2+(\zeta M)^2}{[(-i\omega+\mu)^2-(\zeta M)^2-\omega_c^2n][(i\omega+\mu)^2-(\zeta M)^2-\omega_c^2m]}\end{aligned}$$

$$
\begin{aligned}
&+\frac{n\overline{\omega}_c^2}{\left[(-i\omega_s+\mu)^2-(\zeta M)^2-\omega_c^2(n+1t)\right]\left[(i\omega+\mu)^2-v_z^2p_z^2-\omega_c^2m\right]}\\
&+\frac{m\overline{\omega}_c^2}{\left[(-i\omega_s+\mu)^2-(\zeta M)^2-\omega_c^2n\right]\left[(i\omega_s+\mu)^2-(\zeta M)^2-\omega_c^2(m+1)\right]},\\
S_2=&\frac{\omega_s^2+\mu^2+(\zeta M)^2}{\left[(-i\omega_s+\mu)^2-(\zeta M)^2-\omega_c^2(n+1)\right]\left[(i\omega_s+\mu)^2-(\zeta M)^2-\omega_c^2\right]}\\
&+\frac{\omega^2+\mu^2+(\zeta M)^2}{\left[(-i\omega_s+\mu)^2-(\zeta M)^2-\omega_c^2n\right][(i\omega_s+\mu)^2-(\zeta M)^2]},\\
S_3=&\frac{\left[\omega_s^2+\mu^2+(\zeta M)^2\right]}{\left[(-i\omega_s+\mu)^2-(\zeta M)^2-\omega_c^2\right]\left[(i\omega_s+\mu)^2-(\zeta M)^2-\omega_c^2\right]}\\
&+\frac{\left[\omega_s^2+\mu^2+(\zeta M)^2\right]}{[(-i\omega_s+\mu)^2-(\zeta M)^2][(i\omega_s+\mu)^2-(\zeta M)^2]}.
\end{aligned}
\tag{D14}
$$

The abbreviations are as in 2D, and $v_z \to v_z/T$. For 3D, after performing a summation on the Matsubara frequencies, one finally obtains

$$
\frac{1}{\lambda}=\frac{\zeta\overline{\omega}_c^2}{4\mu^2}\sum_{M>0}\left\{\sum_{n,m}\frac{(m+n)!}{2^{m+n+1}}\frac{f[n]f[m]}{m!n!}s_{nmM}+\sum_n\frac{f[n]f[0]}{2^n}s_{nM}+\frac{f[0]^2}{2}s_M\right\}. \tag{D15}
$$

The summands are as follows:

$$
\begin{aligned}
s_{nmM}=&A\left[\overline{\omega}_c^2(n+1)+(\zeta M)^2,\overline{\omega}_c^2(m+1)+(\zeta M)^2\right]+A\left[\overline{\omega}_c^2n+(\zeta M)^2,\overline{\omega}_c^2m+(\zeta M)^2\right]\\
&+[\mu^2+(\zeta M)^2]\begin{pmatrix}B\left[\overline{\omega}_c^2(n+1)+(\zeta M)^2,\overline{\omega}_c^2(m+1)+(\zeta Mt)^2\right]\\+B\left[\overline{\omega}_c^2n+(\zeta M)^2,\overline{\omega}_c^2m+(\zeta M)^2\right]\end{pmatrix}\\
&+n\overline{\omega}_c^2B\left[\overline{\omega}_c^2(n+1)+(\zeta M)^2,\overline{\omega}_c^2m+(\zeta M)^2\right]+m\overline{\omega}_c^2B\left[\overline{\omega}_c^2n+(\zeta M)^2,\overline{\omega}_c^2(m+1)+(\zeta M)^2\right],
\end{aligned}
\tag{D16}
$$

$$
\begin{aligned}
s_{nM}=&A\left[\overline{\omega}_c^2(n+1)+(\zeta M)^2,\overline{\omega}_c^2+(\zeta M)^2\right]+A\left[\overline{\omega}_c^2n+(\zeta M)^2,(\zeta M)^2\right]\\
&+[\mu^2+(\zeta M)^2]B\left[\overline{\omega}_c^2(n+1)+(\zeta M)^2,\overline{\omega}_c^2+(\zeta M)^2\right]+[\mu^2+(\zeta M)^2]G\left[\overline{\omega}_c^2n+(\zeta M)^2,(\zeta M)^2\right],
\end{aligned}
\tag{D17}
$$

and

$$
\begin{aligned}
s_M=&A\left[\overline{\omega}_c^2+(\zeta M)^2,\overline{\omega}_c^2+(\zeta M)^2\right]+A[(\zeta M)^2,(\zeta M)^2]+[\mu^2+(\zeta M)^2]\\
&\times B\left[\overline{\omega}_c^2+(\zeta M)^2,\overline{\omega}_c^2+(\zeta M)^2\right]+[\mu^2+(\zeta M)^2]B[(\zeta M)^2,(\zeta M)^2],
\end{aligned}
\tag{D18}
$$

with functions A and B given in Appendix B.

[1] E. Helfand and N. R. Werthamer, Phys. Rev. Lett. **13**, 686 (1964).

[2] B. S. Chandrasekhar, Appl. Phys. Lett. **1**, 7 (1962); A. M. Clogston, Phys. Rev. Lett. **9**, 266 (1962).

[3] A. K. Rajacopal and R. Vasudevan, Phys. Lett. **20**, 585 (1966); **23**, 539 (1966).

[4] T. Maniv, A. I. Rom, I. D. Vagner, and P. Wyder, Phys. Rev. B **46**, 8360 (1992); T. Maniv, V. Zhuravlev, I. Vagner, and P. Wyder, Rev. Mod. Phys. **73**, 867 (2001).

[5] M. Rasolt and Z. Tesanovic, Rev. Mod. Phys. **64**, 709 (1992).

[6] Z. K. Liu *et al.*, Nat. Mater. **13**, 677 (2014); B. Q. Lv *et al.*, Nat. Phys. **11**, 724 (2015); Z. K. Liu *et al.*, Science **343**, 864 (2014).

[7] H.-C. Liu, H. Li, Q. L. He, I. K. Sou, S. K. Goh, and J. Wang, Sci. Rep. **6**, 26168 (2016); Y. Zhou, X. Chen, R. Zhang, J. Shao, X. Wang, C. An, Y. Zhou, C. Park, W. Tong, L. Pi, Z. Yang, C. Zhang, and Y. Zhang, Phys. Rev. B **93**, 144514 (2016).

[8] M. Neupane, S.-Y. Xu, R. Sankar *et al.*, Nat. Commun. **5**, 3786 (2014); M. D. Bachmann, N. Nair, F. Flicker, R. Ilan, T. Meng, N. J. Ghimire, E. D. Bauer, F. Ronning, J. G. Analytis, and P. J. W. Moll, Sci. Adv. **3**, e1602983 (2017); Y. H. Zhou *et al.*, Proc. Natl. Acad. Sci. USA **113**, 2904 (2016).

[9] J. Cao, S. Liang, C. Zhang, Y. Liu, J. Huang, Z. Jin, Z.-G. Che, Z. Wang, Q. Wang, J. Zhao, S. Li, X. Dai, J. Zou, Z. Xia, L. Li, and F. Xiu, Nat. Commun. **6**, 7779 (2015).

[10] W. Yu, Y. Jiang, J. Yang, Z. L. Dun, H. D. Zhou, Z. Jiang, P. Lu, and W. Pan, Sci. Rep. **6**, 35357 (2016).

[11] Y. Liu, Y. J. Long, L. X. Zhao, S. M. Nie, S. J. Zhang, Y. X. Weng, M. L. Jin, W. M. Li, Q. Q. Liu, Y. W. Long, R. C. Yu, C. Z. Gu, F. Sun, W. G. Yang, H. K. Mao, X. L. Feng, Q. Li,

W. T. Zheng, H. M. Weng, X. Dai, Z. Fang, G. F. Chen, and C. Q. Jin, Sci. Rep. **7**, 44367 (2017).

[12] S. D. Sarma and Q. Li, Phys. Rev. B **88**, 081404(R) (2013); P. M. R. Brydon, S. D. Sarma, H.-Y. Hui, and J. D. Sau, *ibid.* **90**, 184512 (2014).

[13] B. Rosenstein, B. Y. Shapiro, D. Li, and I. Shapiro, J. Phys.: Condens. Matter **27**, 025701 (2015).

[14] K. W. Song and A. E. Koshelev, Phys. Rev. B **95**, 174503 (2017).

[15] Z. Wang, Y. Sun, X.-Q. Chen, C. Franchini, G. Xu, H. Weng, X. Dai, and Z. Fang, Phys. Rev. B **85**, 195320 (2012).

[16] A. A. Abrikosov, L. P. Gor'kov, and I. E. Dzyaloshinskii, *Quantum Field Theoretical Methods in Statistical Physics* (Pergamon Press, New York, 1965).

[17] D. Li, B. Rosenstein, B. Y. Shapiro, and I. Shapiro, Phys. Rev. B **95**, 094513 (2017).

[18] I. S. Gradshteyn and I. M. Ryzhik, in *Table of Integrals, Series, and Products*, 7th ed., edited by A. Jeffrey and D. Zwillinger, (Academic Press, Burlington, MA, 2007).

[19] S. Jeon, B. B. Zhou, A. Gyenis, B. E. Feldman, I. Kimchi, A. C. Potter, Q. D. Gibson, R. J. Cava, A. Vishwanath, and A. Yazdani, Nat. Mater. **13**, 851 (2014).

[20] I. M. Lifshits, M. Azbel, and M. I. Kaganov, *Electron Theory of Metals* (Consultants Bureau, New York, 1973).

[21] G. Blatter, M. V. Feigel'man, V. B. Geshkenbein, A. I. Larkin, and V. M. Vinokur, Rev. Mod. Phys. **66**, 1125 (1994).

[22] J. Wosnitza *et al.*, Phys. Rev. B **62**, R11973(R) (2000); J. Wosnitza, J. Hagel, O. Ignatchik, B. Bergk, V. M. Gvozdikov, J. A. Schlueter, R. W. Winter, and G. L. Gard, J. Low Temp. Phys. **142**, 327 (2006).

[23] S. Dukan, A. V. Andreev, and Z. Tesanovic, Physica C (Amsterdam) **183**, 355 (1991); S. Dukan and Z. Tesanovic, Phys. Rev. Lett. **74**, 2311 (1995).

[24] Y. Li, Y. Zhou, Z. Guo, F. Han, X. Chen, P. Lu, X. Wang, C. An, Y. Zhou, J. Xing, G. Du, X. Zhu, H. Yang, J. Sun, Z. Yang, W. Yang, H.-K. Mao, Y. Zhang, and H.-H. Wen, npj Quantum Mater. **2**, 66 (2017); B. Q. Lv, H. M. Weng, B. B. Fu, X. P. Wang, H. Miao, J. Ma, P. Richard, X. C. Huang, L. X. Zhao, G. F. Chen, Z. Fang, X. Dai, T. Qian, and H. Ding, Phys. Rev. X **5**, 031013 (2015); H. Wang *et al.*, Sci. Bull. **62**, 425 (2017).

[25] H. Wang, H. Liu, Y. Li, Y. Liu, J. Wang, J. Liu, Y. Wang, L. Li, J. Yan, D. Mandrus, X. C. Xie, and J. Wang, arXiv:1704.00995.

[26] L. Fu and E. Berg, Phys. Rev. Lett. **105**, 097001 (2010).

[27] B. Rosenstein, B. Y. Shapiro, D.-P. Li, and I. Shapiro, Europhys. Lett. **109**, 67006 (2015).

[28] A. A. Soluyanov, D. Gresch, Z. Wang, Q. Wu, M. Troyer, X. Dai, and B. A. Bernevig, Nature (London) **527**, 495 (2015); Y. Sun, S.-C. Wu, M. N. Ali, C. Felser, and B. Yan, Phys. Rev. B **92**, 161107(R) (2015); J. Ruan, S.-K. Jian, H. Yao, H. Zhang, S.-C. Zhang, and D. Xing, Nat. Commun. **7**, 11136 (2016).

[29] M. Alidoust, K. Halterman, and A. A. Zyuzin, Phys. Rev. B **95**, 155124 (2017); G. E. Volovik, JETP Lett. **105**, 273 (2017); arXiv:1701.06435.

[30] R. Y. Chen, S. J. Zhang, J. A. Schneeloch, C. Zhang, Q. Li, G. D. Gu, and N. L. Wang, Phys. Rev. B **92**, 075107 (2015).

[31] L. D. Landau and E. M. Lifshitz, *Quantum Mechanics, Non-Relativistic Theory*, Course of Theoretical Physics, 3rd ed. (Pergamon Press, Oxford, 1977).